

Article

Deciphering Silicification Pathways of Fossil Forests: Case Studies from the Late Paleozoic of Central Europe

Steffen Trümper ^{1,2,*}, Ronny Rößler ^{1,2}  and Jens Götze ³

¹ Museum of Natural History Chemnitz, Moritzstraße 20, D-09111 Chemnitz, Germany; roessler@naturkunde-chemnitz.de

² Institute of Geology, TU Bergakademie Freiberg, Bernhard-von-Cotta-Straße 2, D-09599 Freiberg, Germany

³ Institute of Mineralogy, TU Bergakademie Freiberg, Brennhausgasse 14, D-09599 Freiberg, Germany; jens.goetze@mineral.tu-freiberg.de

* Correspondence: truemper@naturkunde-chemnitz.de

Received: 5 July 2018; Accepted: 26 September 2018; Published: 1 October 2018



Abstract: The occurrence and formation of silicified wood from five late Paleozoic basins in Central Europe was investigated. Fossil wood from diverse geological settings was studied using field observations, taphonomic determinations as well as mineralogical analyses (polarizing microscopy, cathodoluminescence (CL) microscopy and spectroscopy). The results indicate that silicification is either a monophasic or multiphase process under varying physico-chemical conditions. In particular, CL studies revealed complex processes of silica accumulation and crystallization. The CL characteristics of quartz phases in silicified wood can mostly be related to blue (390 and 440 nm), yellow (580 nm), and red (650 nm) emission bands, which may appear in different combinations and varying intensity ratios. Yellow CL is typical for initial silicification, reflecting quick precipitation under oxygen-deficient conditions caused by initial decay of the organic material. Blue CL is predominantly of secondary origin, resulting from replacement of precursor phases by a secondary hydrothermal quartz generation or subsequent silicification of wood. The red CL can be related to a lattice defect (non-bridging oxygen hole center—NBOHC).

Keywords: petrified wood; petrification; cathodoluminescence; quartz; environment

1. Introduction

Both permineralized and petrified plants with preserved cellular details are among the most fascinating remains of the flora and their evolution during Earth history [1–4]. Corresponding fossil occurrences are distributed worldwide in sedimentary and volcanic rocks encompassing million year timespans, beginning with the colonization of the terrestrial realm by higher plants in the Devonian [5] until today's environments, in which ongoing mineralization processes can be observed [6]. There is a large variety of geological settings that yield anatomically preserved plant fossils, their dispersed organs or whole fossil forests preserved in situ. Volcanically-affected landscapes [7], which might be expected to be more prone to rapidly preserve plant remains, are commonly represented in the fossil record. However, in epiclastic sedimentary environments petrifications frequently occur, even in quite unexpected cases, such as low latitude tropical rainforests, which usually show the largest recycling rates of any organic matter [8]. Most permineralized or petrified wood is silicified, viz. preserved by SiO₂ modifications. This may be due to the overall availability of silica as a result of predominating rocks rich in SiO₂ and associated weathering processes.

The desire to decipher the secrets of petrification developed over centuries and has involved manifold attempts and curious experiments. Several questions and phenomena remained so far unexplained, although there is some progress towards understanding single aspects of petrification, e.g., referring to the conspicuous colors found in fossil wood [9] or the steps and mechanisms of fossilization [10,11].

Fundamental studies and experiments [12–15], both under natural conditions and in the laboratory, have contributed towards the understanding of quartz precipitation, plant tissue impregnation and the related time frame [2,16–18]. However, many fossil woods and their occurrences cannot be explained through uniformitarian comparisons, such as postvolcanic hot springs [19,20]. The application of analytical methods, like scanning electron microscopy (SEM) with element contrast imaging by backscattered electrons (BSE) or orientation contrast imaging by electron backscatter diffraction (EBSD), additionally permits a study at the nanoscale of quartz crystallites and their interplay with cell wall structures [21].

Long used successfully in diverse raw material studies and sedimentary petrology [22–25] cathodoluminescence (CL) microscopy also seems a promising approach to analyze silicified wood, because it helps to visualize trace elements or internal textures, such as growth zoning, secondary alteration, or recrystallization [26–28]. Accordingly, the formation history of different quartz generations in fossil wood could be reflected [29–32]. More recently, spatially and time-resolved analysis of CL emission colors and spectra provided new insights into CL variation of silica and its modifications [23,33,34].

The goal of this study is to recognize CL patterns associated with silicification pathways by examining fossil woods preserved in different geological settings. Paleobotanical examination combined with analytical techniques such as polarizing microscopy, cathodoluminescence (CL) microscopy, and spectroscopy, as well as scanning electron microscopy (SEM), are applied.

2. Material and Methods

Specimens investigated during this study are stored in the Paleontological Collection of the Museum für Naturkunde Chemnitz (K2097, K6556, K6562, K6563), except for one, which belongs to the Museum für Naturkunde Berlin (1977/7). The Chemnitz collection represents a remarkable set of anatomically preserved plant fossils from different sites worldwide and encompasses material from various geological settings and stratigraphic levels [35]. In this approach, the focus is on silicified wood-bearing localities, which have been investigated recently by the authors in the field and under the microscope. Additionally, any comparisons and discussions of the selected localities benefit from their well-known geological settings and stratigraphy both in a regional and global context [36].

Samples were documented macroscopically by using a Nikon D5300 digital camera, and microscopically by using NIS-Elements D (version 3.2) software under a Nikon SMZ 1500 microscope (all Nikon Cooperation, Tokyo, Japan). Thin sections were investigated under plane-polarized (PPL), cross-polarized transmitted light (XPL) and cathodoluminescence (CL). CL analyses were carried out on polished standard thin sections which were coated with carbon in order to prevent any build-up of electrical charge during CL operation. The thin (ca. 5 nm) carbon layer ensures transparency for both transmitted light and CL observations, and has no influence on the microscopic investigations. The CL microscope was a “hot cathode” CL microscope HC1-LM (designed by U. Zinkernagel and modified by R. Neuser at the Ruhr-University, Bochum, Germany), which used an acceleration voltage of 14 kV and a beam current of 0.2 mA [37]. CL images were taken with an Olympus DP72 digital camera (Olympus Cooperation, Tokyo, Japan). CL spectra in the wavelength range of 370–900 nm were recorded with an Acton Research SP-2356 spectrograph (Princeton Instruments, Acton, MA, USA), linked to the microscope via an optical glass-fiber guide. CL spectra were recorded under standardized conditions with a spot size of about 30 μm in diameter by using a pinhole aperture. An Hg-halogen lamp was used for wavelength calibration. The measured CL spectra are presented as curves in wavelength-CL intensity diagrams. Due to the light diffraction, a CL spectrum results from interference of CL signals

derived from an area larger than the spot. Accordingly, a spectrum contains several CL signals caused by different defect structures in the corresponding silica phases.

3. Geological Setting

3.1. Late Paleozoic Environments Capable of Preserving Silicified Woods

Petrified wood dating back to the late Paleozoic is known from numerous localities in Central Europe, covering a wide range of lithologies and depositional settings (Figure 1). This abundance and diversity is connected to climatic and geotectonic conditions in tropical central Pangaea, which were conducive for wood petrification. Initiated by climatic change from tropical ever-wet to subtropical seasonally wet conditions from the late Moscovian into the Permian (Figure 2), wood-forming gymnosperms (i.e., cordaitaleans, conifers) flourished and expanded from extra-basinal areas prone to erosion, to the basin centers [38,39]. Contemporaneously, late- to post-collisional collapse of the Variscan Mountains in Central Europe facilitated the formation of closely arranged intramontane basins, where fossils were preserved [40,41]. Rapid denudation filled the newly formed accommodation space with thick, predominantly siliciclastic successions [42]. Syndepositional explosive volcanism using intersecting faults as conduits favored rapid burial of plants, including the entombment of entire ecosystems known as “T⁰ assemblages” [7,43,44].

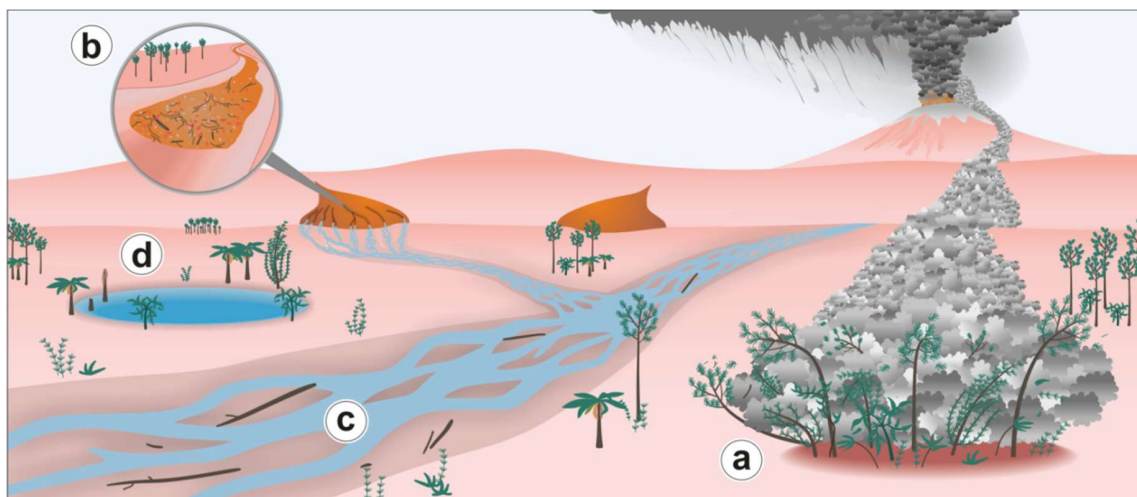


Figure 1. Petrified-wood forming environments of the late Paleozoic in Central Europe. (a) In situ burial in pyroclastic deposits (Flöha, Wendishain, Chemnitz). (b) Alluvial transport and burial by mass flows with/without volcanic material (Winnweiler). (c) Reworking and burial of stems in fluvial deposits (Kyffhäuser). (d) Silicification in lacustrine and palustrine environments (Manebach).

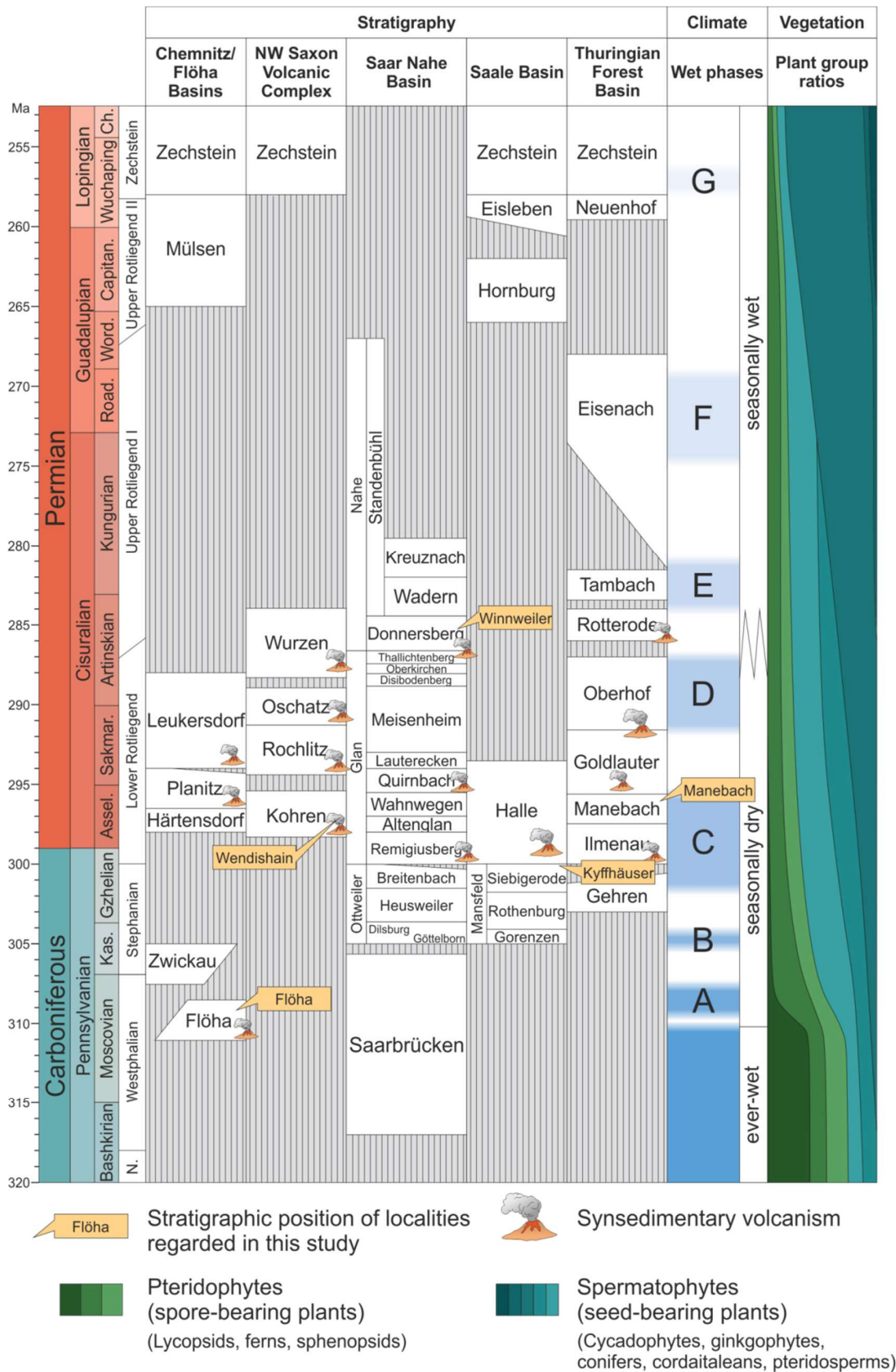


Figure 2. Lithostratigraphy of selected late Paleozoic intramontane basins. Tectonic basin formation around the Carboniferous-Permian boundary is accompanied by volcano-sedimentary deposits and abundant hiati in the stratigraphic record. From the middle Pennsylvanian onwards, gradual aridization favored the expansion and diversification of seed-bearing plants including wood-forming gymnosperms (conifers, cordaitaleans, ginkgophytes). Compiled and modified after [36,44–46]. Vegetation data are based on [38,39,47] and personal observations.

3.2. Sampling Locations of Investigated Silicified Woods

The positions of the investigated occurrences of silicified wood in Central Europe are presented in Figure 3.

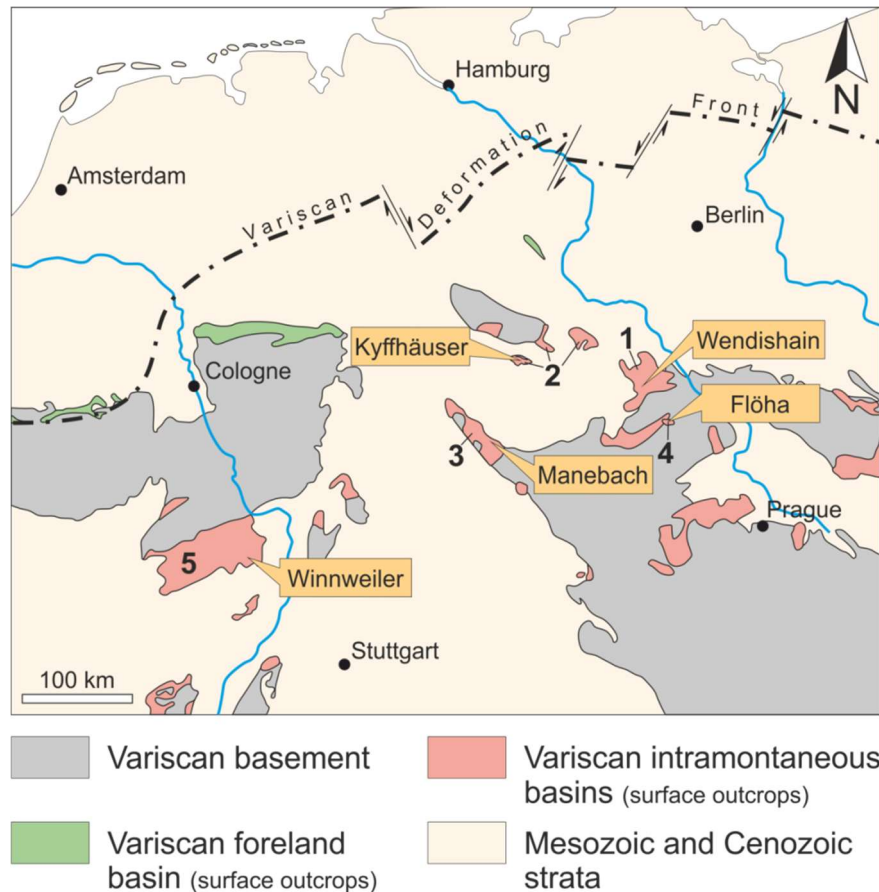


Figure 3. Generalized geological map of Central Europe showing the position of the selected localities. Modified after [48]. 1—NW Saxon Volcanic Complex; 2—Saale Basin; 3—Thuringian Forest Basin; 4—Flöha Basin; and 5—Saar-Nahe Basin.

Sample K6563 was found in Holocene colluvial sediments of the Struth Forest near Falkenau, located in the foreland of the Erzgebirge in East Central Germany. Based on the adhering rock, the stem was originally embedded in sediments accompanying the Schweddey Ignimbrite of the late Carboniferous Flöha Formation (Moscovian, Flöha Basin, Figures 2 and 3). This feldspar-rich pyroclastic rock is attributed to a pyroclastic density current entombing and fragmenting late Carboniferous coal-forming vegetation including woody trunks [49–51]. The age of the Schweddey Ignimbrite was recently constrained to 310 ± 2 Ma based on radiometric U/Pb measurements obtained from different outcrops, and a Bolsovian macroflora [49,50,52].

Sample K6562 from Wendishain is derived from a 48×40 cm sized block containing an incomplete silicified stem section measuring 30×40 cm in diameter, and its adhering pyroclastic host rock. This block was found parautochthonously on a field in Wendishain. The adhering rock consists of a greenish wood-bearing quartz-rich ignimbrite. Based on reworked lithics derived from the Leisnig Porphyry, the stem was originally embedded in the topmost up to 10 m thick beds of the Kohren Formation (Asselian, NW Saxon Volcanic Complex, Figures 2 and 3) overlying the Leisnig Porphyry. The Kohren Formation recorded deposition by alluvial fans, meandering rivers and lacustrine to palustrine sediments in abandoned channels and swamps, accompanied by syndimentary volcanism [53–55].

Sample K6556 from Winnweiler was removed directly from alluvial volcano-clastic deposits of the Donnersberg Formation (middle to late Artinskian, Saar-Nahe Basin, Figures 2 and 3). Its sediments reflect deposition in alluvial fans, braided and meandering rivers, including associated floodplains, within the half-graben like Saar-Nahe Basin [56]. Synsedimentary volcanism resulted in the formation of voluminous subvolcanic, effusive, pyroclastic, and epiclastic rocks [57]. The silicified wood-hosting strata at Winnweiler are of low maturity with respect to sediment composition and texture. The poorly sorted and non-stratified wood-bearing debrites range from coarse-grained pebbly sandstones to sandy conglomerates accompanied by high contents of clay and silt in the matrix. The matrix may be red or light green in color, and contains reworked tuffaceous material.

Sample K2097 was found allochthonously in alluvial fan deposits formed at the northern margin of the Kyffhäuser SW of Tilleda during the Pleistocene. Silicified woods at Tilleda are derived from pebbly, fine- to coarse-grained quartz arenites of the Siebigerode Formation (latest Gzhelian, Saale Basin, Figures 2 and 3) [58–61] exposed in the Kyffhäuser. These log-bearing sandstones are highly mature with respect to composition, expressed by quartz contents ranging from 70 to 90% volume. The Siebigerode Formation reflects deposition in medium- to large-scaled braided rivers [59,62]. Wood logs derived from extrabasinal areas were transported in the fluvial system during floods, and subsequently settled on barforms [59].

Sample 1977/7 has been found in colluvial deposits derived from uphill outcrops of the Manebach Formation (Asselian, Thuringian-Forest Basin, Figures 2 and 3) in the Schulzental valley close to Manebach. The up to 200 m thick, greyish Manebach Formation shows a diverse lithology, comprising fluvial channel sandstones, *Scoyenia*-bearing siltstones, lacustrine claystones, hydromorphic paleosols, palustrine coals, and silicified peats [63,64]. Its host rock represents silicified peat intercalated in sandstones and conglomerates. The Manebach Formation is correlated climatostratigraphically with the late Carboniferous-early Permian wet phase C (Figure 2). Silicified plants from Manebach recently attracted scientific attention due to the exceptional preservation of fungal endophytes, epiphytic ferns and pteridosperms, as well as coprolites of parasitic arthropods within their tissues [65,66].

4. Results

4.1. Flöha

The specimen is a 7 cm long fragment, and possesses an oval shape in cross-section measuring 9.5×5.5 cm in diameter (Figure 4b,c). Anatomically, the stem only consists of wood showing a green color (Figure 4c–g). The latter is caused by a green mineral phase occupying the former cell walls or partially filling the cell lumina (Figure 4e).

Silicification is promoted by clear quartz filling the cell lumina (Figure 5a). Quartz crystals are restricted to 1–4 tracheids (Figure 5b). The wood is variably preserved, i.e., disintegrated into single cells (Figure 5d), plastically deformed (Figures 4g and 5d), or fractured (Figure 4f,g and Figure 5d,e). In areas of appropriate anatomical preservation, the 28 to 50 μm wide cells are oval to polygonal in cross section d,e, and Figure 5a,b, and point to a cordaitalean affinity. Under CL, the silicified wood predominantly displays a short-lived blue CL (Figure 5c,f). Spectral measurements (Figure 5g) show that the blue band is very broad and consists of at least two overlapping component bands centered at 390 and 450 nm. Due to the spectral range of the analytical arrangement, the 390 nm band is only visible as a shoulder in the CL spectra. After three minutes of irradiation, CL intensity decreases by 60% (Figure 5g). Next to blue luminescent areas, yellow CL (main emission band at ca. 570 nm) and red CL (main emission band at 650 nm) occur randomly within the cell lumina (Figure 5c,e,f). Areas of blue CL on the one hand, and yellow and red CL, on the other hand, do not differ with regard to anatomical preservation.

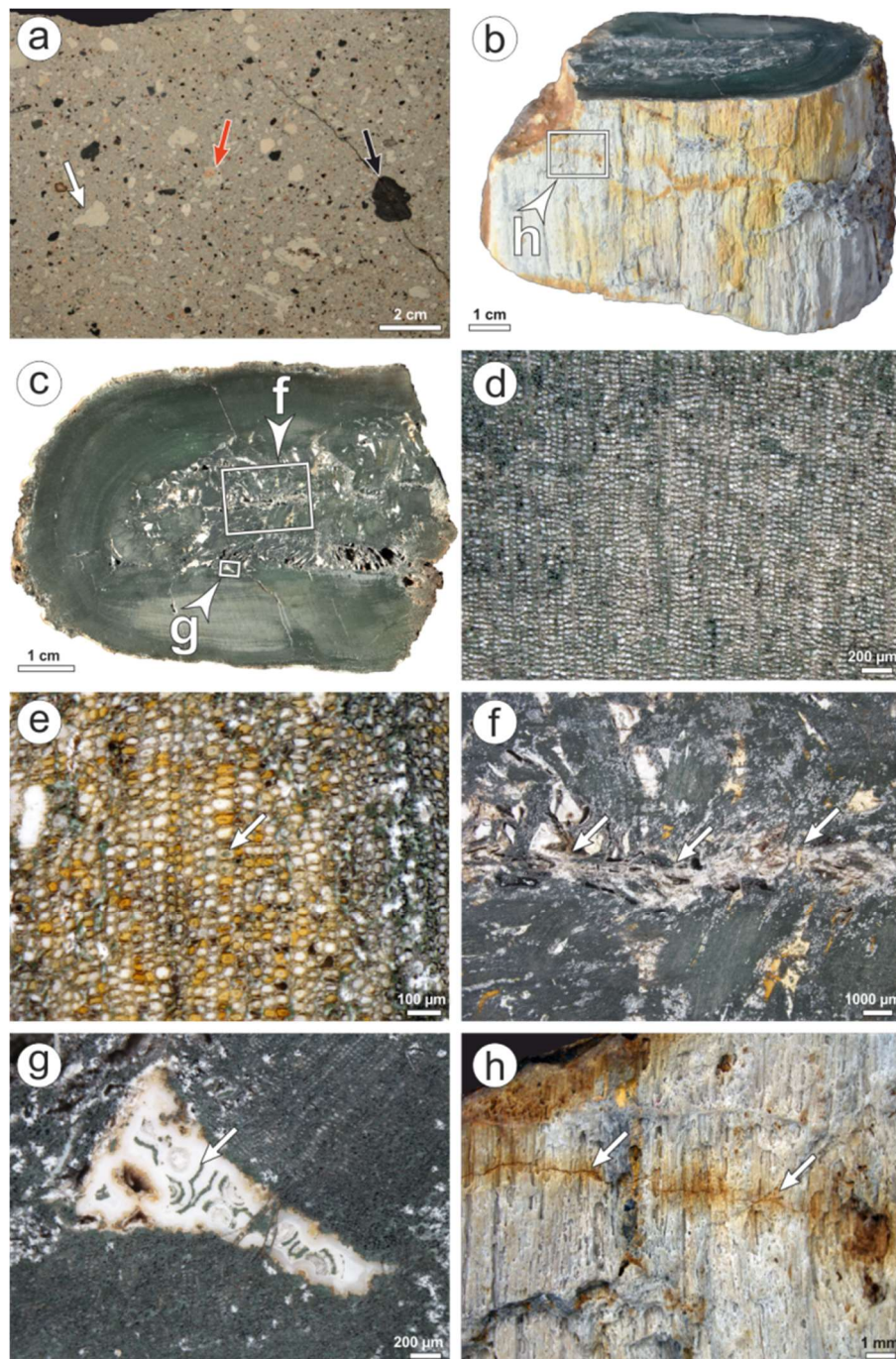


Figure 4. Features of K6563 and the Schweddey Ignimbrite from Flöha. (a) Schweddey Ignimbrite, containing carbonized plant remains (black arrow), weakly welded pumice (white arrow) and cm-sized feldspars (here plagioclase incorporating an orthoclase, red arrow). (b) Stem, from which K6563 is derived from. (c) Stem in cross section. Note the inner part of the stem showing abundant cavities filled by white agate. (d) Green-colored wood in cross section. (e) Close-up of the wood showing polygonal shapes of the tracheids in cross-section. Cell walls and parts of the cell lumina (arrow) are filled by a green mineral phase. (f) Close-up of the stem's center. The former pith cavity is compressed to a white line (arrows). (g) Cavity filled by white agate. Note intercalations of a green mineral phase (arrow). (h) Limonite-bearing fractures (arrows) as pathways for oxidation caused by weathering.

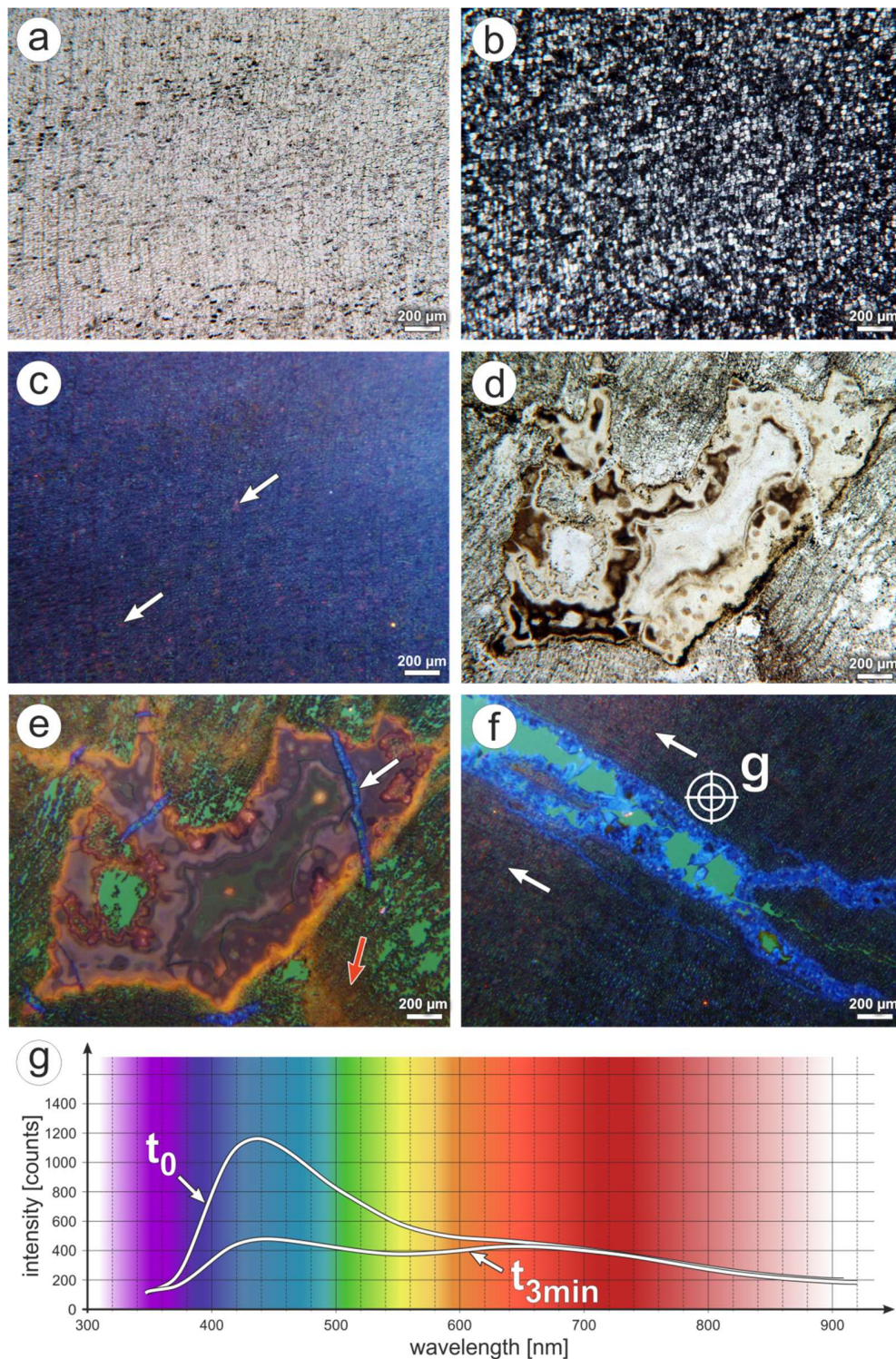


Figure 5. CL of K6563. (a) Silicified wood; PPL image. (b) Same view as in (a); XPL image. Note that quartz crystals comprise single tracheids or tracheid groups. (c) Same view as in (a), CL image, showing a short-lived blue CL interspersed with centers of red CL (arrows). (d) Agate-filled cavity; PPL image. (e) Same view as in (d); CL image. The agate possesses a brown CL, whereas surrounding intercellular space is filled by green-luminescing epoxy. Fillings of tight fractures dissecting the agate have a blue CL (white arrow). Neighboring areas show a yellow CL (red arrow). (f) Fracture filled by euhedral quartz displaying a short-lived blue CL; CL image. Note diffusively occurring red CL in cell lumina (arrow). (g) CL spectra taken at (f). Note decreasing intensity of blue CL after three minutes of irradiation, whereas red CL remains constant.

From inwards outwardly, the center is characterized by a 30 mm long line orientated parallel to the stem's largest diameter (Figure 4f), and resulted from pith compression. It is surrounded by a 1.5 cm thick zone of inner wood showing abundant cavities, each a couple of millimeters in length (Figure 4c,f). The cavities are empty or filled by white agate, and are aligned sub-parallel to the stem's smallest diameter (Figure 4c,f,g). Internally, the agate shows a concentric layering, often accompanied by intercalations of the green mineral phase (Figure 4g). In places, botryoidal structures can be observed. Fragmented wood files occurring in isolation within the cavities are encrusted by agate layers. Under CL, the agate shows a reddish-violet CL (Figure 5e). Along cavity margins, orange CL can be observed (Figure 5e). As a special feature, the agate-filled cavities are dissected by 100 μm wide fractures filled by quartz. These fractures end at the edge of the agate-filled cavities, and show a short-lived blue CL (Figure 5e). Wood around the cavities is disintegrated. The intercellular space is exclusively filled by epoxy, derived from thin section preparation and reveal intense, homogeneous green CL (Figure 5e).

The outer wood, a 2 cm thick zone, lacks any agate-filled cavities (Figure 4c). Radially aligned, up to 0.5 mm wide fractures occurring here are incompletely filled by euhedral quartz blades rooting at the fracture-wood interface (Figure 5f). This euhedral quartz shows a short-lived blue CL identical to fillings in fractures occurring within agate-filled cavities (Figure 5f). Along fractures and across the surface of K6563, hematite formation reflects oxidation probably connected to weathering (Figure 4h).

It should be mentioned here in addition that silicified wood from other outcrop areas of the Schweddey Ignimbrite (e.g., the Oderan Forest site) show a short-lived blue CL throughout the wood.

4.2. Wendishain

The rock adhering to the stem consists of crystals, wood fragments, pumice, and volcanic lithics in order of decreasing abundance, embedded in a green-colored cryptocrystalline siliceous matrix (Figure 6a). The rock is non-stratified and poorly sorted and, thus, is classified as ignimbrite. The crystal content comprises angular to splintery, 1 or 2 mm large quartz crystals displaying a short-lived blue CL at 440 nm (Figure 7a), and black, columnar amphibols. The angular, pale-green to violet wood fragments range in diameter from 3 mm to 2.5 cm. The white pumice fragments are poorly welded, and reach sizes of a couple of millimeters up to 3 cm (Figure 6a). Lithics are restricted to less than 2.6 cm large red volcanics showing abundant altered feldspars, amphibols, and rare quartz (Figure 6a). The matrix is cryptocrystalline and revealed a short-lived blue CL (Figure 7a).

The stem possesses an intensive orange to red color and comprises a sector of the originally complete diameter, which is supposed to have represented ca. 70 to 90 cm (Figure 6b). Anatomically, this fragment only consists of wood, and adjoins the embedding pyroclastic rock with an uneven, but macroscopically sharp interface (Figure 6c). Internally, the stem displays a color zonation, comprising three zones. From outside inwards, there is a greyish-white to rose-colored, 0.5 to 2 cm thick zone 1, followed by a predominant 14 to 20 cm thick red to orange zone 2 showing grey dots, and a dark-grey to brown zone 3 (Figure 6c,d). A thin section of K6562 has been cut from the margin, comprising the embedding tuff and zones 1 and 2. Color zonation is barely reflected in the anatomical preservation both macroscopically and microscopically. The wood's preservation shows cell walls being diffusely outlined under transmitted light (Figure 6e). However, cells are more clearly recognizable under CL. Silicification is promoted by coarse crystalline to cryptocrystalline quartz (Figure 6f,g).

On a microscopic scale, there is a fluent transition from ignimbrite to wood, based on gradual disintegration of the tissue (Figure 6e). Silicified wood from zone 1 displays a time-dependent CL, being initially blue (decreasing 450 and 390 nm bands), and turning into red (increasing emission band at 650 nm) (Figure 7b). Fracture fillings consisting of coarse-crystalline quartz are almost non-luminescent (Figures 6g and 7c,d). Towards zone 2, initially blue CL of the cell walls is gradually replaced by yellow CL (emission band at ca. 570 nm) in areas distant to fractures (Figure 7c,d). In zone 2, finally, cell walls have a yellow CL, and cell lumina are characterized by red to brown CL (main CL emission band

around 650 nm) (Figure 7e,f). Fractures in areas transitional to zone 1 and within zone 2 are filled by cryptocrystalline silica showing a reddish-brown CL similar to the surrounding wood (Figure 7f).

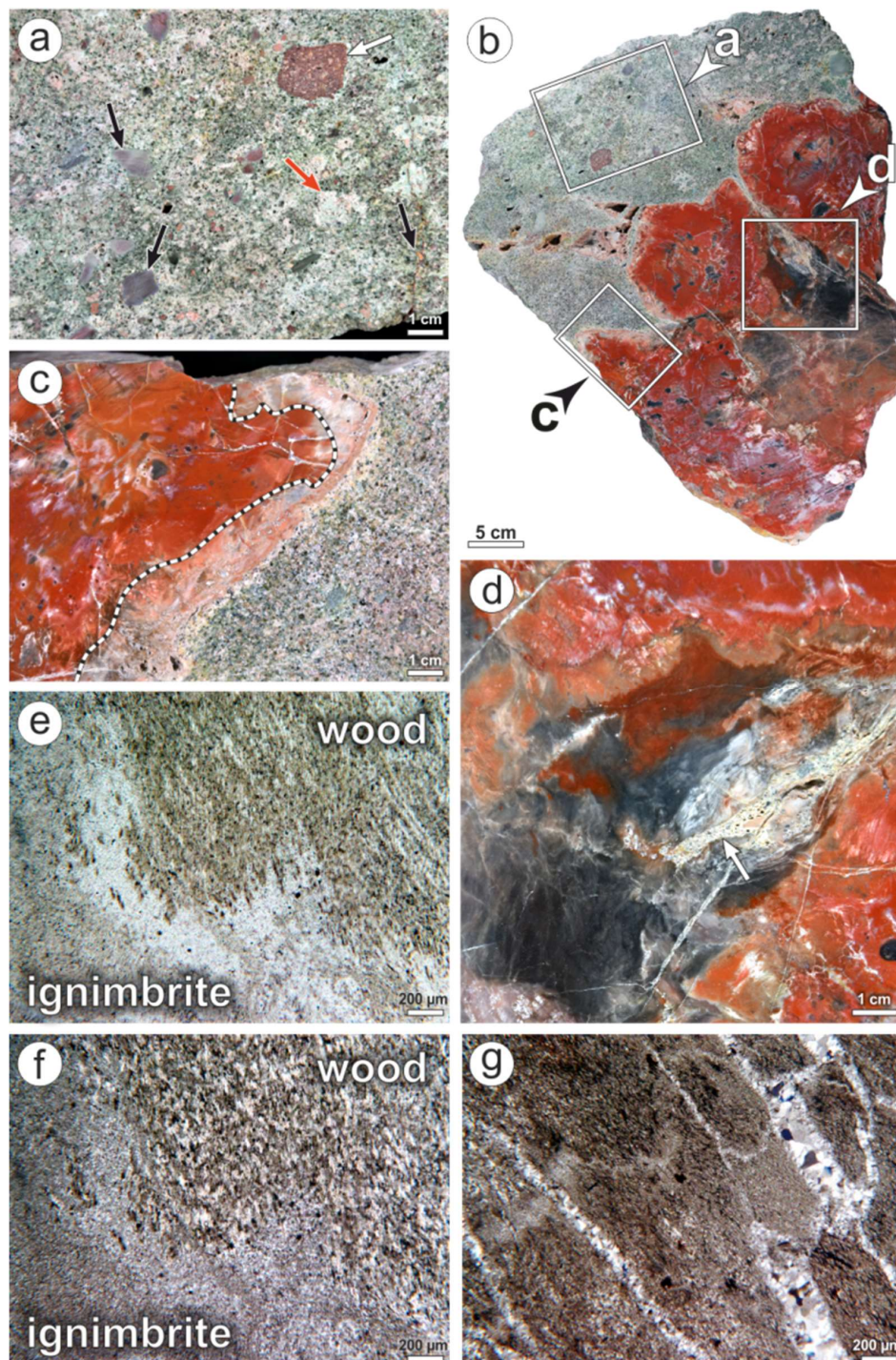


Figure 6. Features of K6562 and its host rock from Wendishain. (a) Ignimbrite consisting of wood fragments (black arrows), pumice (red arrow) and lithics (white arrow). (b) Cross-section showing silicified wood (red) with adhering ignimbrite (green). (c) Color zonation of the wood with an outer greyish-white to rose-colored zone 1, and an inner orange zone 2 (dotted line as border). (d) Color zonation of the wood with orange zone 2, and dark grey to brown zone 3. Note fracture fillings with ignimbrite (arrow). (e) Gradual transition from wood into ignimbrite; PPL image. (f) Same view as (e); XPL image. (g) Zone 2; XPL image. Note coarse-crystalline quartz in the fractures.

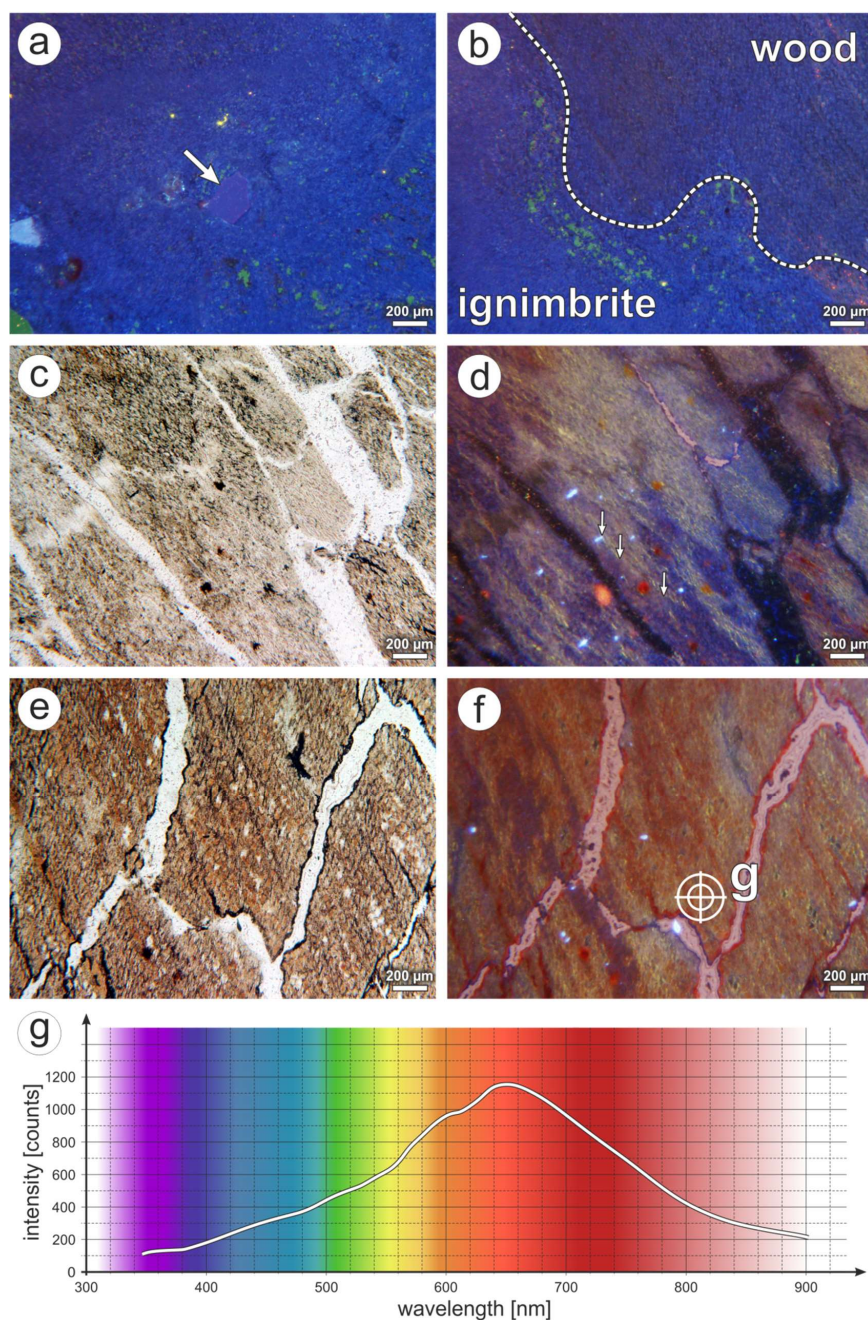


Figure 7. CL of K6562. (a) CL image of the ignimbrite showing short-lived blue CL of the matrix and a quartz grain (arrow). (b) Same view as in 8e; CL image. Note identical CL of both wood in zone 1 and ignimbrite. (c) Transition of zone 1 and 2 PPL image. (d) Same view as in (c); CL image. Yellow CL is restricted to areas distant to fractures (arrows). (e) Zone 2; PPL image. (f) Same view as in (e); CL image. Note that blue CL has been replaced by red CL in the cell lumina. Fractures are filled by red-luminescent cryptocrystalline silica. (g) CL spectrum taken at (f).

4.3. Winnweiler

K6556 contains a 2.9 cm thick silicified wood. It consists of two xylem strands but lacks any pith. Based on the aforementioned anatomical characteristics, the wood is identified as a gymnosperm root. The root is embedded in a matrix made up of 0.2 to 2 cm large wood fragments, red chalcedony, pale agate and calcite in order of decreasing abundance (Figure 8b,d). In general, silicified wood occurs in two preservation types, which can also be distinguished by their CL: (1) anatomically well preserved showing yellow and red CL (emission bands at 580 and 650 nm, respectively; Figures 8d,e and 9a–d),

and (2) anatomically poor-preserved displaying a short-lived blue CL (Figures 8f–h and 9e,f). The first type is limited to the innermost 20 mm of the gymnosperm root. Here, cells are preserved without visible deformation (Figures 8e and 9a). The tracheids possess a circular cross cut, and decrease in diameter from 64 μm in the root's center to 39 μm in the outer wood (Figure 8d). According to [67], a coniferophyte origin can be assumed. The general decline of tracheid diameter is superimposed by rhythmic variations of tracheid diameters and wall thicknesses, reflecting some kind of concentric growth zonation (Figure 8d). In general, the inner part of the root exposes different CL, each of them showing a more or less distinct spatial distribution (Figure 9c,d). Red CL is predominantly restricted to silica either filling cell lumina or incompletely covering the inner surface of fractures running through the wood (Figure 9c). Rarely, both cell lumina and walls show a red CL. By contrast, yellow CL is strictly limited to the former cell walls (Figure 9c). Areas characterized by yellow and red CL merge laterally into such being almost non-luminescent (Figure 9d).

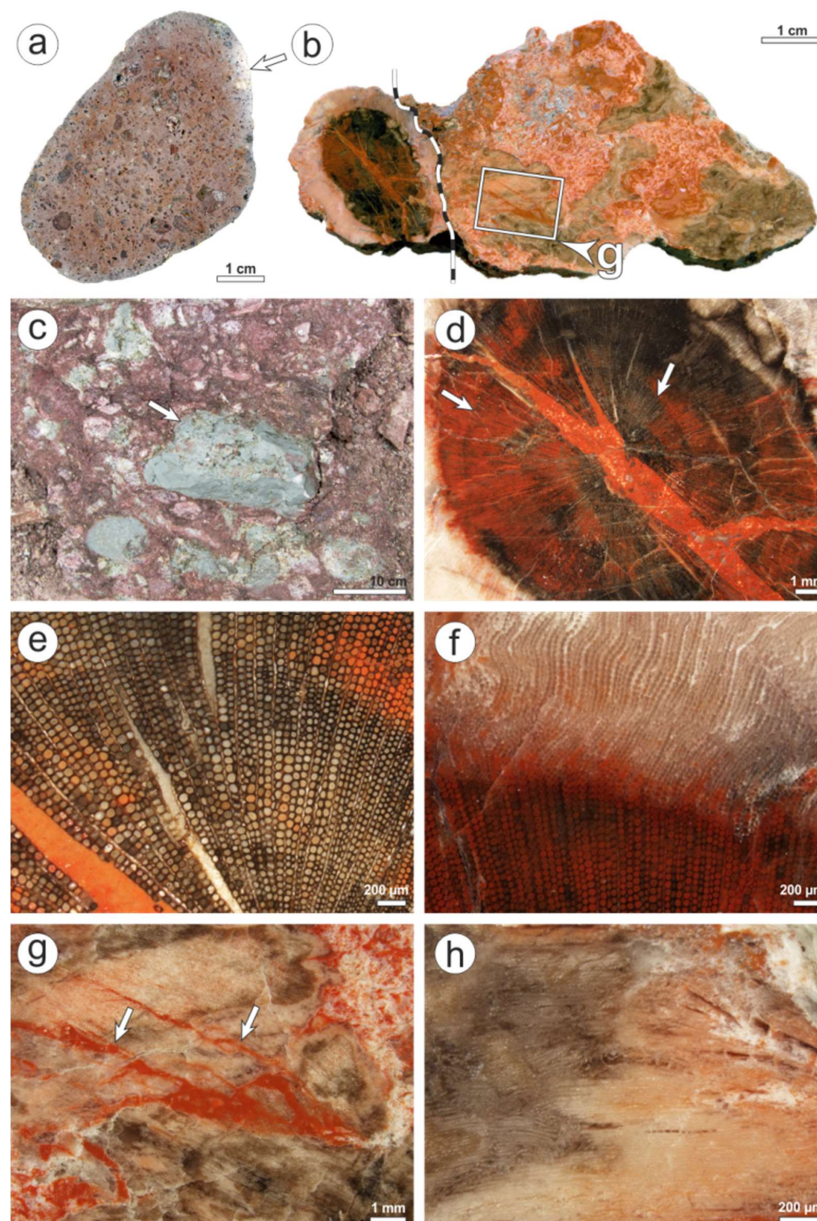


Figure 8. Features of K6556 and its host rock from Winnweiler. (a) Rhyolite clast from alluvial debris of the Donnersberg Fm. Note roundness and bleaching (arrow). (b) K6556. The dotted white line marks

the interface of the root cross-cut (left) and the surrounding matrix containing wood fragments (right). (c) Typical debris of the middle Donnersberg Fm. Note crucial features of alluvial mass flows: missing sorting and bedding, and polymict composition with lithics (here green tuffs; arrow). (d) Close-up of the inner root in cross-section showing growth zonation. (e) Round-shaped tracheid cross-cuts. (f) Border of well-preserved inner root (below) and poor-preserved outer root rim (above). (g) Close-up of wood fragments surrounding the root. Note the jigsaw-like match of neighboring fragments (white arrows). (h) Frayed wood in the matrix surrounding the root.

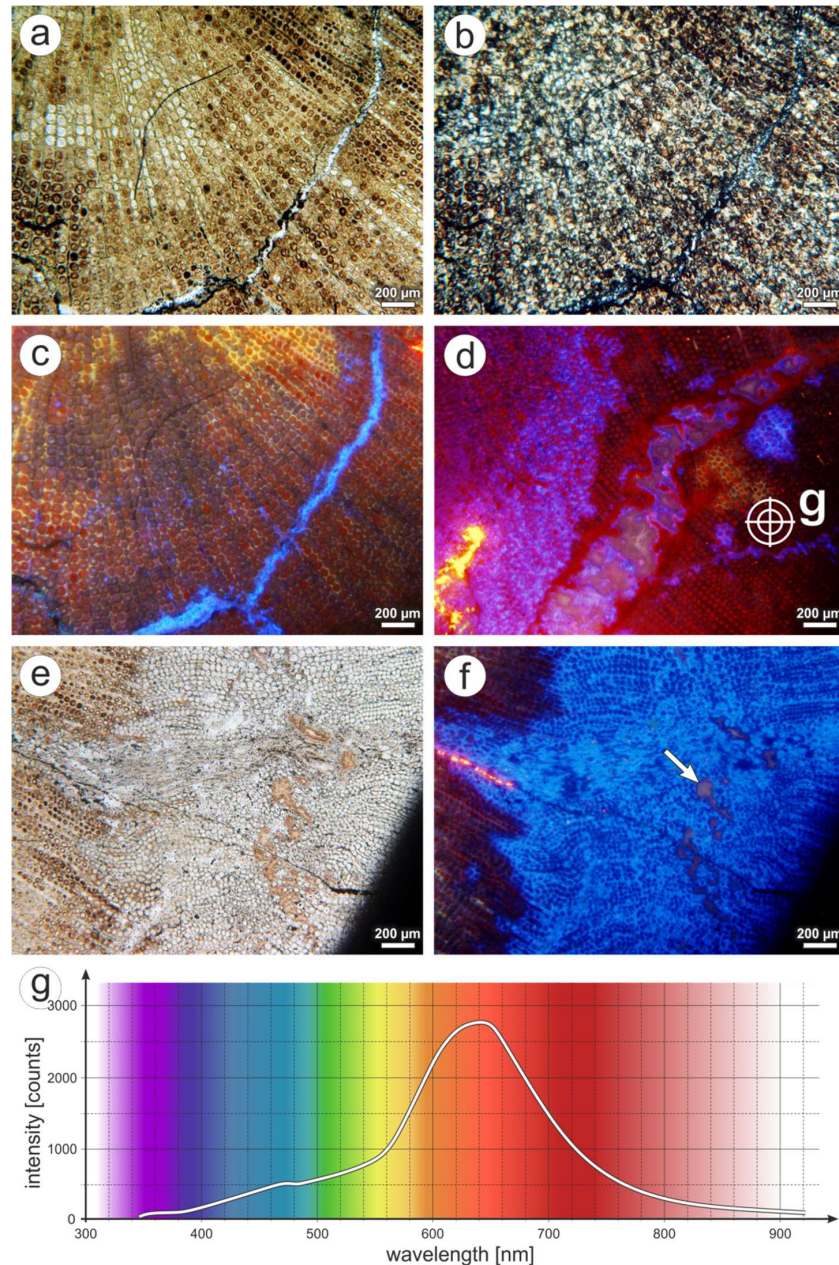


Figure 9. CL of K6556. (a) Anatomically well-preserved wood of the inner part of the root (type 1; PPL image). (b) Same view as in (a); XPL image. (c) CL image of (a). Note limitation of yellow CL to the former cell walls, whereas red CL occurs within the cells. Fracture filling shows a short-lived blue CL. (d) All CL spectra detected in K6556; image taken from the inner root. Note that anatomical preservation within irregularly shaped occurrences of short-lived blue CL is lower than around. (e) Anatomically poor-preserved wood of the outer rim of the root (type 2; PPL). (f) CL image of (e). Brown-luminescing agate fills holes in the wood (arrow). The occurrence of short-lived blue CL is strictly connected to cellular preservation. (g) CL spectrum taken at (d).

Type 2 showing a short-lived blue CL is demonstrated in the following parts of K6556: (1) fractures running radially and concentrically through the wood in the inner part of the root (Figure 9c), (2) irregularly to circular-shaped patches of the wood within the inner part of the root (Figure 9d), (3) the approximately 10 mm thick outer rim of the gymnosperm root (Figure 9f), and (4) wood fragments surrounding the root. Anatomical preservation is generally weak, as indicated by highly deformed cells (Figure 8f–h). In places, the wood is disintegrated into tracheid rows and even single tracheids (Figure 8h). Irregularly, but sharply shaped holes within type-2-silicified wood are filled by brown-luminescing agate (Figure 9f).

A couple of tracheids along the outer margin of the root, as well as fractures within, are completely or partially filled by calcite indicated by intense orange CL (emission band at 620 nm; Figure 9d,f).

4.4. Kyffhäuser

K2097 (Figure 10d) is a fragment of silicified *Agathoxylon*-type wood showing the typical “pointstone preservation” of Kyffhäuser specimens. In cross section, the eponymous “points” are circular to oval or rhombic, darkish brown areas of silicified wood, ranging from 1.5 to 3 mm in diameter (Figure 10e). If non-circular in shape, the “points” are orientated with their largest diameter in a radial or tangential direction. Within the “points”, preservation of cell structures follows a gradient. Non-deformed cells and well recognizable cell walls only occur in the innermost area, which encompasses approximately one-third to one-half of the “point’s” complete diameter (Figures 10g and 11a). Here, each former cell is occupied by one quartz crystal, which may be either transparent or milky and macroscopically opaque (Figure 11b). In some “points”, a concentric alternation of transparent and milky cell lumina fillings resulted in the formation of rings (Figures 10e and 11a,c). In contrast to the “point’s” center, cells in the outermost part are sheared, resulting in oval shapes (Figures 10f,h and 11a). Cell walls are blurred, but still act as boundaries for quartz crystals, which—in contrast to the innermost area—cover two or three cells instead of one. Concerning CL, the “points” exhibit a weak yellow CL (main emission band at 580 nm, Figure 11c). As a feature special to Kyffhäuser woods, such areas are strewn with 50 µm large dots, showing a much more intense yellow to orange CL. These dots occur separately, but also rarely form clusters of two or three dots (Figure 11c,e,f).

The “points” either occur as tight clusters (Figures 10d and 11d), or are separated from each other by transparent, fine- to macro-crystalline quartz (e.g., having grain sizes of 0.5 to 3 mm; Figure 10d–f). In the latter case, the “points” are surrounded by radially aligned euhedral quartz blades. In these quartz blades, increasing deformation of cell structures, which starts in the outermost area of the “points”, culminates in herringbone-like arrangements of poorly preserved cell walls (Figure 10f,h and Figure 11a,b). With increasing distance to the “points”, quartz crystals become anhedral, clear and free from any cell structures.

Areas of crystalline quartz in between the “points”, where anatomical preservation is low or cells are not present, are characterized by intense, short-lived blue CL resulting in non-luminescence after a few minutes irradiation (Figure 11e,f).

In a longitudinal section, the previously described “pointstone preservation” appears as a banded structure (Figure 10f). Hence, the “points” just represent two-dimensional cross-cuts of actually spheroidal to tube-like petrification bodies.

Conspicuously, the previously described anatomical and CL features can be observed in silicified woods from other localities situated in the Siebigerode Formation across the whole Saale Basin, e.g., Siebigerode and Wettin, which are located 28 km or 52 km, respectively, NE of the Kyffhäuser.

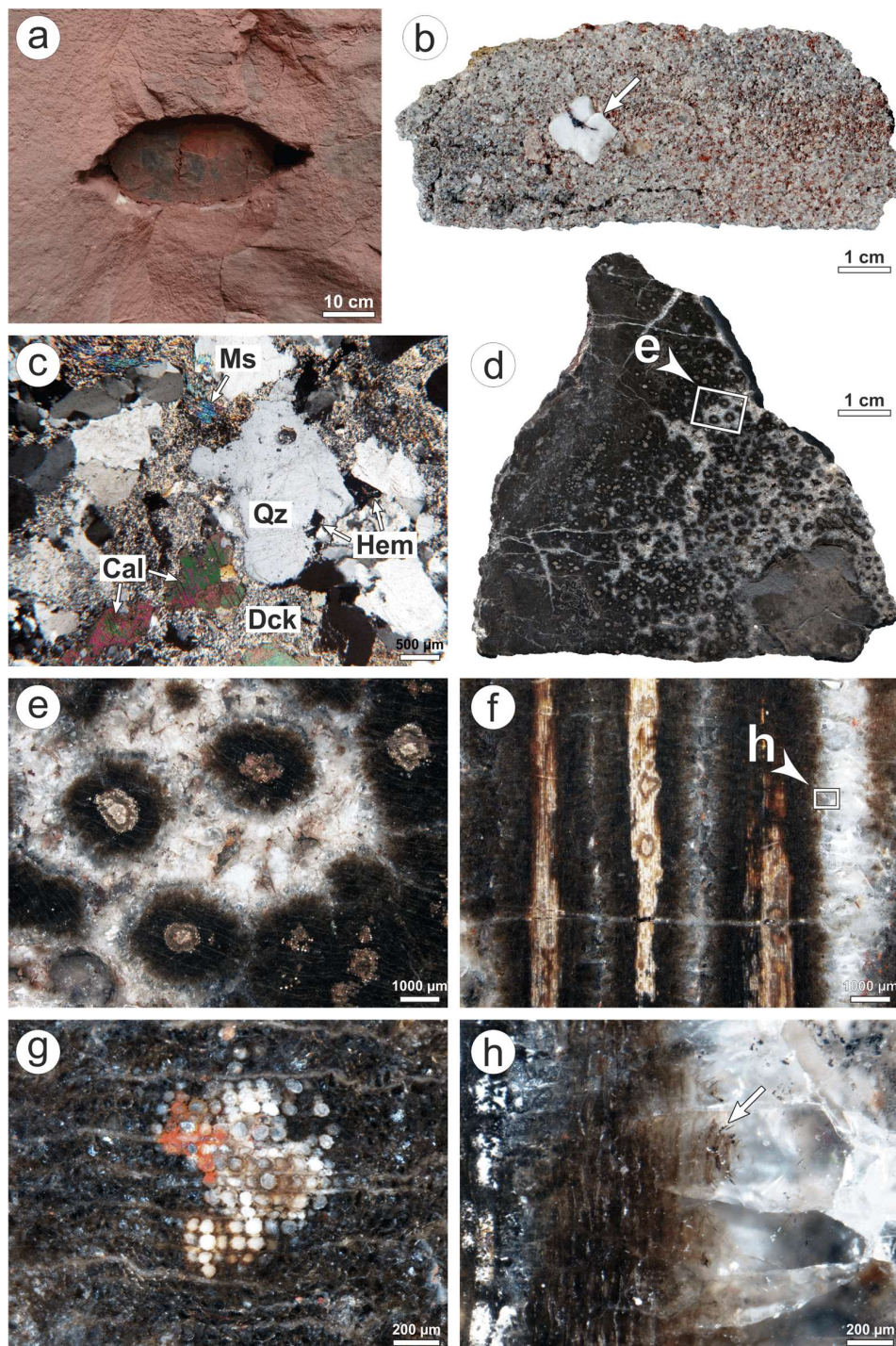


Figure 10. Features of K2097 and its host rock from the Kyffhäuser. (a) Appearance of logs in the field: cross-cut of a log horizontally embedded in medium-grained sandstones. Note vertical compaction by oval geometry of the cross-cut. (b) Typical reddish white kaolin sandstones of the Siebigerode Fm. The log-bearing fine- to medium-grained sandstones are mostly well sorted and only contain rarely pebbles (arrow). (c) XPL image of B showing the mineralogical composition of the sandstones: quartz (Qz) and muscovite (Ms) as detrital grains, whereas intergranular space is filled by dickite (Dck), calcite (Cal) and hematite (Hem) in order of decreasing abundance. (d) Cross-cut of silicified *Agathoxylon*-type wood preserved as “pointstone”. (e) Close-up of the “points”. (f) “Pointstone” preservation in longitudinal section revealing a tube-like or spheroidal geometry. (g) Center of a “point” in cross-section. Note the increasing deformation from the center outwardly. (h) Close-up of F showing large quartz blades, which incorporate plastically deformed wood cells.

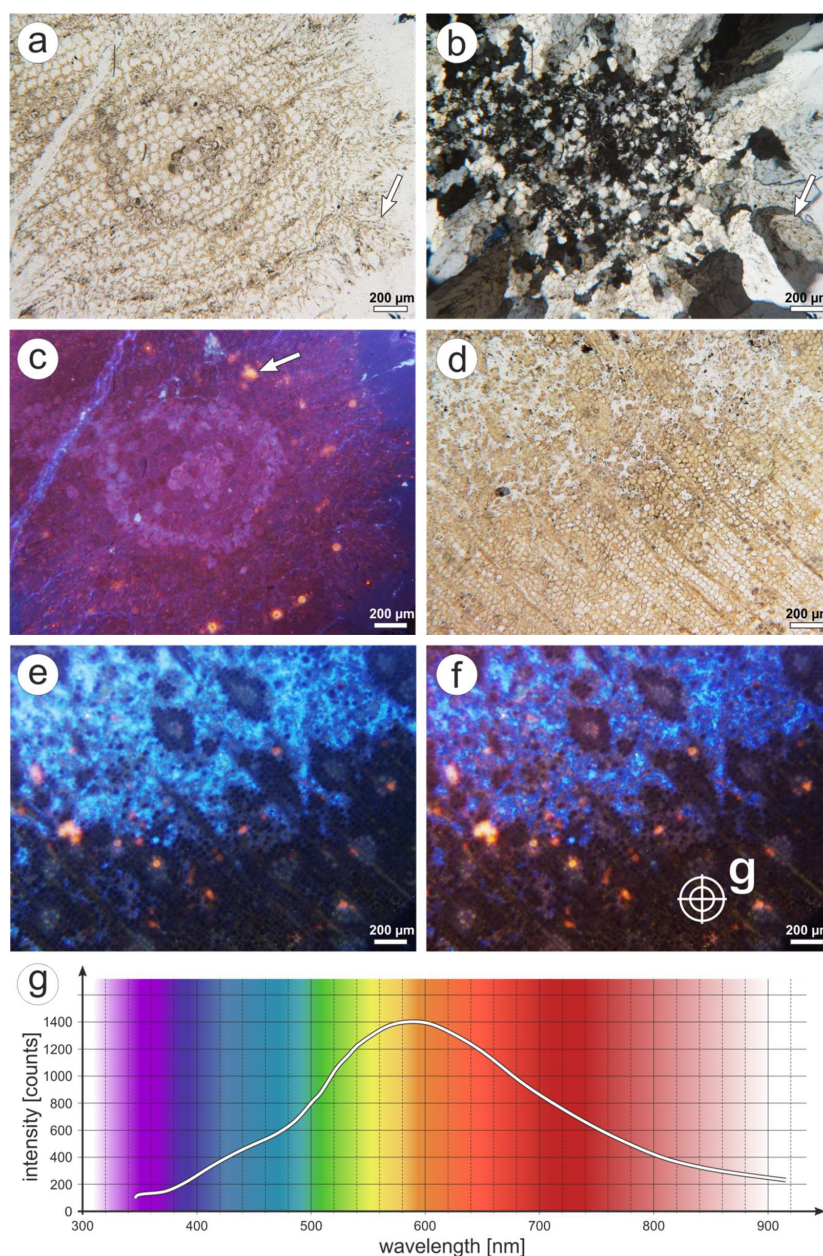


Figure 11. CL of K2097. (a) “Point” in PPL. Note highly deformed cells surrounding the “point” (arrow). (b) Same view as in (a); XPL image. Each cell is occupied by one quartz crystal in the inner part of the “points”. (c) Same view as in a; CL image. The macroscopically visible rings yield different CL intensities under CL. The “point” is rich in yellow halos (arrow). (d) “Pointstone” fabric; PPL image. (e + f) Same views as in (d). CL images taken initially (e) and after three minutes of irradiation (f). Note decreasing intensity of blue CL in between the “points”. (g) CL spectrum taken at (f).

4.5. Manebach

1977/7 consists of an *Agathoxylon*-type stem, 2.5×3.5 cm in diameter, which is encrusted by a 1.2 cm thick stromatolite (Figure 12b). In cross section, the stem is almost complete, but lacking bark and pith (Figure 12c). The wood is permineralized, and its black color resulted from preserved carbon in the former cell walls (Figures 12d and 13a). Radial tracheid walls are covered by biseriate pits (Figure 12d). Cell lumina are filled with white silica, which appears to be homogeneous under polarized transmitted light. CL images of the cell fillings, however, reveal two different emission types: a first type with predominant, low-intense, time-dependent blue-red CL, and a second type with more

or less stable yellow CL (emission band around 580 nm; Figure 13c–e). The first type is visually almost non-luminescent because of the low CL intensity, but extended exposure times and spectroscopic measurements reveal initial dark blue CL, gradually shifting to red (increasing 650 nm band) after three minutes of irradiation. Areas of yellow CL occur randomly, without apparent connections to wood anatomy or cellular preservation.

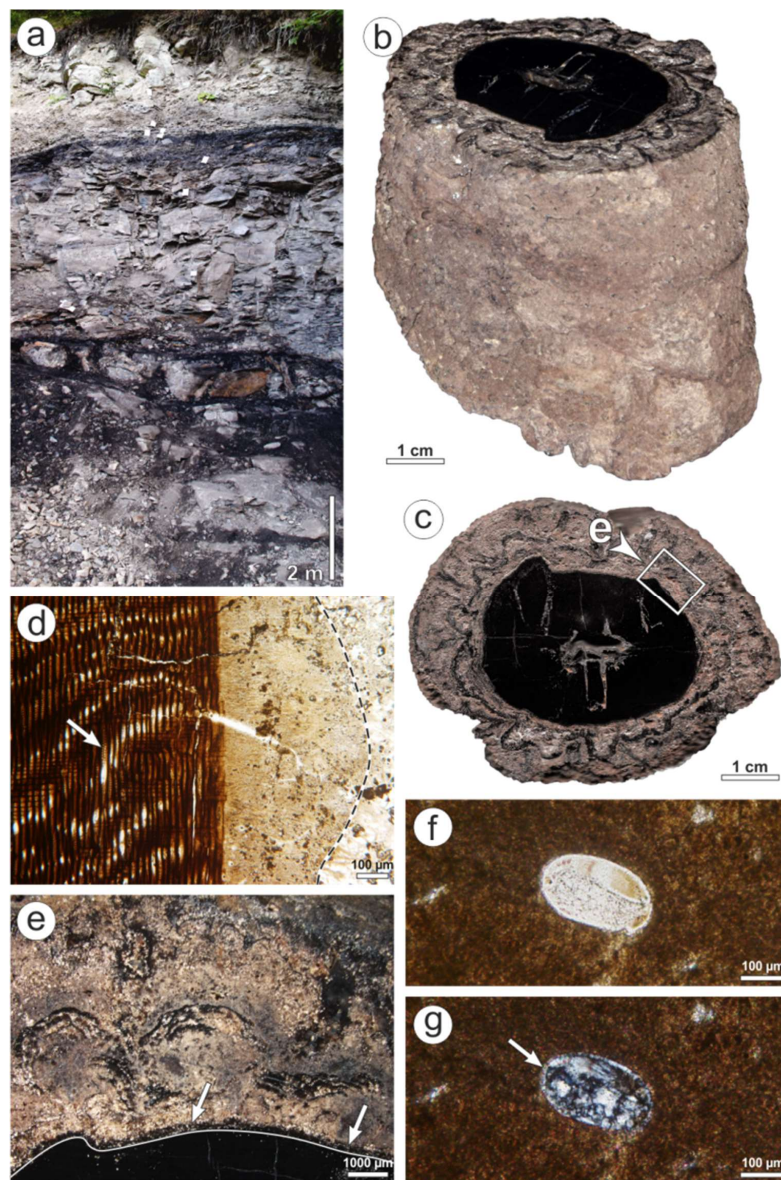


Figure 12. Features of 1977/7 and its host rock from Manebach. (a) Typical section of the Manebach Fm. showing a vertical succession of floodplain siltstones (grey), fluvial sandstones (pale yellow) and intercalated coal seams (black). (b) Permineralized *Agathoxylon*-type stem, encrusted completely by a stromatolite; lateral view (1977/7). (c) Cross-section of B. Note the uniform thickness of the stromatolitic mantle. (d) Interface of stem (left) and silicified stromatolite (right); radial view; PPL image. Exceptional preservation in Manebach is reflected by delicate anatomical features, such as pits in the tracheids (arrow), and microbial filaments in silicified parts of the stromatolite (left of the dotted line). (e) Interface of permineralized stem (black) and stromatolite. Whereas calcite prevails in the stromatolite, silicification is limited to single black laminae, and a fringe around the stem (arrows and continuous line). (f) Ostracod within the stromatolite; PPL image. (g) Same as (f); XPL image. The ostracod is completely filled by quartz, which also replaced calcite in the shell. Residual calcite is indicated by interference colors of higher orders (arrow).

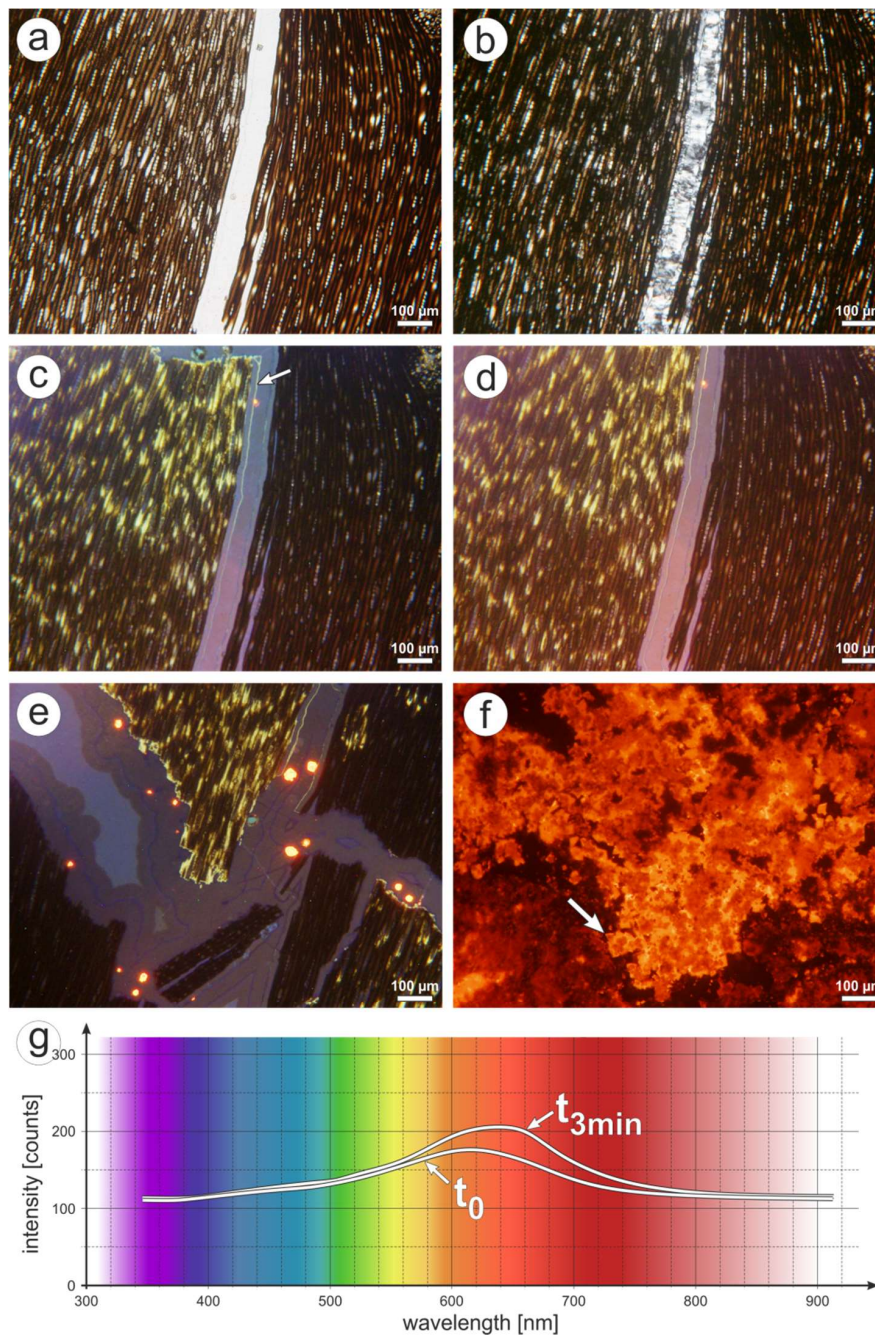


Figure 13. CL of 1977/7. (a) Radial section of the wood; PPL image. A longitudinally aligned fracture separates the wood along the tracheids. (b) Same photo as in (a); XPL image. Due to the strong inherent color of the organically preserved cell walls, the wood appears brown. The fracture is filled by two generations of quartz. (c) Initial CL image of a. The wood left of the fracture shows a yellow CL, whereas the fracture filling and the wood on the right side display a low intensity blue CL. Different generations of quartz within the fracture are indicated by yellow CL along their interface (arrow). (d) CL image after three minutes of irradiation. Note the shift to a red CL, whereas yellow CL is comparatively stable. (e) Initial CL image of a fracture dissecting the wood. The fracture filling is rich in less than 50 μm large calcite crystals showing an intense orange CL at 620 nm. (f) Initial CL image of the calcareous stromatolite encrustation, which is made up of 30 μm large euhedral calcite crystals (arrow). (g) CL spectra of silica showing a lowly intense, time-dependent color taken initially (t_0) and after three minutes of irradiation (t_{3min}). Each curve resulted from interference of three different luminescences: blue (440 nm), yellow (580 nm; diffracted radiation from neighboring areas) and red (650 nm). Note increasing intensity of red CL with time.

Up to 1 mm wide fractures, crossing the wood in longitudinal direction, are filled with one or two silica generations (Figure 13a–e). Surprisingly, all generations show the same CL, and belong to the time-dependent first type. In CL images, different generations of fracture fillings can only be distinguished by their borders, which possess a yellow CL similar to type two (Figure 13c). As a striking feature, the silica within the fractures encloses isolated, 10 to 70 μm large, subhedral or anhedral calcite crystals (Figure 13e).

The wood borders on the stromatolite with sharp contact (Figure 12d). The stromatolite is predominantly calcified, but also partially silicified. Silicifications are either limited to single stromatolithic laminae, or occur as a 300 μm thick fringe around the stem (Figure 12e). Figure 12d shows the fringe in radial section, in which microbial filaments still seem to be obvious. In contrast to silicified parts of the stromatolite, calcified parts do not exhibit any microbial structures. Calcite forms aggregates of up to 50 μm large rhombohedral crystals (Figure 13f). In places, calcified parts of the stromatolite contain up to 0.5 mm large ostracods, either occurring in cavities within the stromatolite, or being completely encrusted (Figure 12f). They are preserved with both valves still in occlusion and, therefore, point to life positions. Even if completely encrusted by calcified stromatolite, the ostracods are completely silicified, including their shell. Rarely, relic calcite can be recognized (Figure 12g).

5. Discussion

5.1. Specific Characteristics of the Silicified Wood Localities

5.1.1. Flöha

Petrified wood from Flöha shows a three-phase silicification. After sedimentation, a quick first-phase silicification promoted by hydrothermal fluids, most likely connected to the Schweddey Ignimbrite, affected the wood throughout the whole stem. This process is reflected by randomly distributed blue, yellow, and red CL of the corresponding quartz. Silicification was interrupted or accompanied, respectively, by deposition of the green mineral phase within the wood. Given the abundance of the same green mineral phase in the originally vitreous, nowadays clayish matrix of the Schweddey Ignimbrite [49,50], a clay mineral affiliation can be suggested. The green color points to reduced iron, which is typical for clay minerals of the mica, smectite, and/or chlorite groups.

Clay mineral deposition was accompanied by agate formation, which is reflected by intercalations of green clay minerals and white agate in cavities (Figure 4g). Both represent the second phase of silicification. The third and last phase of silicification affected fractures formed both in the wood and in agate-filled cavities. This last phase was initiated by hydrothermal fluids.

Silicification was preceded by sedimentation and mechanical compaction of the stem due to pith degradation. Compression of the horizontally embedded stem resulted in the formation of cavities, which represent fractures aligned sub-parallel to the direction of compaction. These processes were followed by a multiphase silicification, given variously luminescing quartz in the wood, agate-filled cavities and fractures dissecting the wood (Figures 4 and 5).

The **first phase of silicification** was accomplished by quartz precipitation in the wood. A clear chronological order of the differently luminescing parts cannot be deduced based on the random distribution of yellow and red CL (Figure 5c,e,f). Additionally, a synchronous formation of blue-, yellow- and red-luminescing quartz should not be excluded. In particular, the short-lived blue CL and the yellow CL are typical for quartz formed from aqueous solution under low-temperature hydrothermal conditions [25,27]. Accordingly, the observed luminescence characteristics reflect quick silicification accompanied with hydrothermal fluids during the first phase of silicification.

Based on the observation that green clay minerals filled the remaining space in the cell lumina left from quartz precipitation (Figure 4e), indicates clay mineral impregnation following on the first phase of silicification. Additionally, based on the occurrence of clay minerals in the former cell walls (Figure 4d,e), the organic framework may still have existed during first-phase silicification. Afterwards, organic components were apparently decomposed and replaced by clay minerals. This process

was accompanied and followed by agate formation in cavities, as intercalations of clay minerals within botryoidal agate suggest (Figure 4g). Hence, agate formation represents the **second phase of silicification** and reflects quick precipitation under high silica concentrations [33].

Silicification ceased with the formation of fractures both in the wood and in the agate-filled cavities (**third phase of silicification**; Figure 5e,f). By providing pathways for hydrothermal silica-bearing fluids, these fractures were filled by euhedral quartz (Figure 5f).

5.1.2. Wendishain

Petrified wood from Wendishain displays a two-phase-silicification. After burial by a pyroclastic flow, the embedding ignimbrite provided silica at high concentrations resulting in rapid first silicification of the complete stem. Whereas cell lumina were filled by red-luminescing silica, local oxygen deficiency in the cell walls resulted in the formation of yellow CL. Contemporaneously, or shortly afterwards, agate precipitation in fractures occurred. A second phase promoted by hydrothermal silica-bearing fluids entering the stem via fractures followed. Fractures were filled by coarse-crystalline quartz being almost non-luminescent.

A chronological order of formation of the differently luminescent silica phases cannot be deduced from preservation quality only. The fact that short-lived blue CL in the wood is limited to its outer margin bordering the ignimbrite (zone 1; Figure 7b), or to halos around fractures (Figure 9d), suggests a secondary origin of blue-luminescing silica. Consequently, red and yellow luminescing areas of zone 2 have to be regarded as representing the **first phase of silicification**, whereas short-lived blue CL displays a second phase of silicification.

Yellow and red CL of the silica phases reflect rapid precipitation from supersaturated solutions during the **first phase of silicification** [23,34,68]. This process was accompanied by local oxygen deficiency, as yellow CL of the former cell walls suggests (Figure 7d,f) [34]. Fractures were synchronously, or shortly afterwards filled, by red-luminescing agate (Figure 7f), displaying rapid precipitation from supersaturated solutions [33]. Conditions for first-phase silicification may be provided by alteration of the embedding ignimbrite.

Relict agate-filled fractures in blue-luminescing wood of zone 1, as well as yellow-luminescing cell walls in wood transitional from zone 1 to zone 2 (Figure 7d) indicates that, originally, the stem was completely affected by first-phase silicification. This is supported by an almost equal level of anatomical preservation throughout the stem (Figure 6e,g). **Second-phase silicification** has started at the outer margin of the stem, and penetrated the already silicified tissue afterwards via fractures. This process was accompanied by restructuring of the silica lattice and incorporation of alkali-compensated $[\text{AlO}_4/\text{M}^+]$ centers responsible for blue CL [25,27]. The observed time-dependent CL shifting from blue to red CL emission is typical for silica formed from hydrothermal solutions [23].

5.1.3. Winnweiler

CL analysis of K6556 from alluvial deposits of the Donnersberg Formation revealed a two-phase silicification, followed by calcification. During the first phase of silicification, intact wood characterized by wider tracheids was silicified rapidly under oxygen deficiency resulting in yellow and red CL. The second (hydrothermal) phase affected still non-silicified parts of the wood, which prior to that have been subjected to advanced decomposition. Agate was precipitated finally in holes left in the wood. Petrification finished with calcite formation in some tracheids, and within fractures crossing the wood. Given the composition and low permeability of the embedding epiclastic rocks, alteration of volcanogenic material is regarded as the probable source of the silica at the Winnweiler locality.

According to both preservation types observed in K6556, which also show a different CL, a two-phase silicification can be assumed. A first phase, which was restricted to the inner anatomically well-preserved part of the root (type 1), and a second phase, which affected the anatomically poorly preserved outer rim of the root and surrounding wood fragments (type 2).

The well-preserved tissues in the central part of the root indicate a negligible degree of decomposition during the **first phase of silicification**. Yellow and red CL of the corresponding silica phases (Figure 9c,d) refer to rapid precipitation at high concentrations of silica and oxygen deficiency [34,68]. The spatial separation of both luminescence types—red CL of silica filling cell lumina and fractures, and yellow CL of the former cell walls (Figure 9c)—may indicate an asynchronous formation of both, and thus sub-phases within first-phase silicification. However, which CL—the red or yellow one—was formed first, cannot be answered based on the data observed in K6556.

Widespread plastic deformation of wood cells showing a short-lived blue CL (Figure 9e,f) suggests an advanced state of decomposition during the **second phase of silicification**. Such features would not be preserved in case of an origin of the blue-luminescing silica by replacement or recrystallization of pre-existing silica phases. Consequently, an initially incomplete impregnation or silicification of the wood must be assumed. As silica impregnation of wood depends, amongst other things, on the tracheid diameter [23,69], first-phase silicification of the root's interior could have been favored by its wider tracheids. Short-lived blue CL indicates the origin of the silica from hydrothermal solutions [23,28]. Finally, holes in the wood left from hydrothermal silicification after the second phase were filled by agate showing a red to brown CL (Figure 9f). Red to brown CL is abundant in cryptocrystalline silica [23,33], and points to precipitation from supersaturated solution [33]. Calcification is regarded as final stage of wood petrification.

5.1.4. Kyffhäuser

Results point to a two-phase silicification for the Kyffhäuser logs. Silica precipitation was initiated by reducing, acidic conditions within the decomposing wood after burial. However, as initial impregnation of the wood with silica was incomplete, first-phase silicification was limited to single tracheids, where anatomical preservation therefore is best. Wood decomposition was faster than silicification, resulting in gradients of anatomical preservation nowadays known as “pointstone preservation”. The model explains abundant vertical compaction of logs in the Kyffhäuser section, which is a consequence of sediment burden of decomposing, slowly silicifying wood in a highly aggrading fluvial system [59]. Silicification was completed by hydrothermal precipitation of quartz showing a short-lived blue CL in empty spaces left from decomposition and fractures in the wood.

CL proves a two-phase silicification of woods from the Kyffhäuser: one phase characterized by yellow CL, and another characterized by short-lived blue CL. However, which phase occurred first is reflected by anatomical preservation. As cell structures are best-preserved within the “points”, silicification certainly started there, suggesting that the yellow luminescing areas represent the **first phase**. After initial silicification of single tracheids in the center of the later “points”, silicification must have propagated into the surrounding wood tissue. This is supported by gradually decreasing anatomical preservation from the center of the “points” outwardly. Ongoing silicification was accompanied by simultaneous degradation of the still non-petrified wood tissue, mirrored by plastic deformation of cell walls due to probable lignin decomposition. Wood decomposition is in accordance with yellow CL of the corresponding quartz, which—according to [34,68]—is connected to rapid crystallization under conditions of oxygen deficiency and high concentrations of silica. Anyway, both anatomical preservation and yellow CL indicate reducing conditions within the buried wood, which stands in contrast to oxidizing conditions in the embedding hematite-bearing, originally permeable sediments. Reducing conditions were probably accompanied by low pH values, given the fact that oxygen-deficiency favors the formation of organic acids in decomposing wood. A reducing, acidic environment facilitates the precipitation of silica in the wood. Besides SiO₂, uranium was probably mobilized and accumulated within the wood material. The characteristic, up to 50 μm large radiation halos developed around radioactive inclusions within the silica due to radiation damage [70,71]. However, the first phase of silicification ceased from formation of radially aligned quartz blades around the “points”. At this time, wood decomposition had progressed enough, that quartz could grow euhedrally and permeate and shear residual wood tissue.

The **second phase** of silicification affected the space in between the “points”, as well as fractures crossing the wood. The observed short-lived blue CL is typical for a hydrothermal origin [28,34]. Contrary to the first phase, any wood at places of second-phase silicification has already been decomposed completely prior to quartz crystallization.

5.1.5. Manebach

Sample 1977/7 revealed two types of the occurring silica phases with yellow, and a time-dependent low-intensity CL, respectively. The CL signatures point to silicification from hydrothermal solutions [23,28]. The occurrence of yellow CL in between the other quartz generations indicates changing physico-chemical conditions during silicification (Figure 13c).

However, both luminescence types indicate a silicification by hydrothermal fluids, which must have occurred quite early and rapidly, given the yellow CL and the following reasons: 1. the generally exceptional preservation (Figures 12d and 13a); 2. the organic preservation of tissues [11], including the potential for preserving delicate endophytic fungi [66]. Moreover, silica precipitation is supposed to have been accomplished under stable conditions, which is reflected by several quartz generations in fractures with identical CL (Figure 13c,e), and the overall homogeneous CL found in other samples.

Silicification of the stem followed on from stromatolite formation. This is supported by silica fringes around the silicified stem (Figure 12e), isolated calcite crystals completely enveloped by silica in fractures of the wood (Figure 13e), and the replacement of calcite by silica in ostracod shells (Figure 12g). Additionally, observations by [72] on recent caldera lakes prove the preservation of microbial filaments in siliceously preserved stromatolites as being typical for a secondary silicification. Stromatolite formation must have affected the stem in growth position, as the uniform thickness of the encrustation suggests (Figure 12c). Additionally, lacking bark and pith refer to the stem as being already dead during stromatolite formation. Whether the death of the stem was connected to flooding prior to stromatolite formation cannot be answered with certainty. It should, however, be noted that early conifers of the late Paleozoic preferred dry sites. Accordingly, conifers are comparably rare elements in floral assemblages of the fluvial Manebach Fm. [73].

The taphonomic pathway for 1977/7 can be reconstructed as follows: (1) Death of the tree, accompanied by loss of both the bark and the pith tissues; (2) flooding of the still upright tree and in situ encrustation with stromatolites; (3) rapid silicification of the stem and partial replacement of calcite by silica in the stromatolite; and (4) entombment of the stem. The results point to in situ calcification with subsequent silicification of upright stems in hydrothermal ponds or lakes.

5.2. General CL Characteristics of Silicified Wood

The localities regarded in this study generally suggest that wood silicification can be accomplished as a monophasic (Manebach), or multiphasic (Flöha, Wendishain, Winnweiler, Kyffhäuser) process. A biphasic silicification appears to be the most common case. These observations are reflected in other studies [29–31] and are already indicated by different silica generations and modifications visible under transmitted light. Silica in petrified wood displays only a small number of CL colors, comprising the composite blue (390 and 440 nm), yellow (580 nm), and red (650 nm) emission bands. Other studies [29–31,74] found a similar range, except for very rare occurrences of green CL [31]. Hence, petrified wood CL is apparently less diverse than luminescences identified in quartz-bearing sedimentary, magmatic, and metamorphic rocks, and hydrothermal veins, in general [23,29]. However, blue CL in the considered localities is restricted to micro- and macrocrystalline quartz, whereas both microcrystalline (quartz) and cryptocrystalline silica varieties (agate, chalcedony) can additionally display yellow and red CL. Similar CL was observed in previous studies [29–31,74].

With respect to petrified woods from the late Paleozoic in Central Europe (this study; [29–31,74]), parts of the wood affected by initial silicification exclusively show yellow and/or red luminescences. Especially the formation of yellow luminescing silica appears to be inevitable in early silicification, given the occurrence of yellow CL in all selected localities and depositional settings. This observation

could be connected to the fact that oxygen-deficient organic decay is always present in recently buried wood. Both yellow and red CL point to initial silicification as being rapid and derived from supersaturated silica-bearing fluids under low-thermal (<250 °C) conditions [23,29,34].

Blue luminescing silica in petrified wood is predominantly of secondary origin, i.e., formed by later crystallization in fractures or non-silicified wood (Winnweiler, Flöha, Kyffhäuser, Hawk Mountains/Intrasudetic Basin according to [74]), or replacement of precursing phases (Chemnitz/[29], Wendishain, Flöha). Amongst the investigated localities, Manebach (and nearby localities occurring in the Manebach Formation, e.g., Crock) is exceptional as blue CL forms part of the first phase of silicification.

5.3. Occurrence-Specific CL Characteristics of Silicified Wood

First of all, CL characteristics of petrified wood can be specific either to a locality, or to certain taphonomic circumstances (i.e., host rock/depositional environment). The discrimination of both factors requires a good taphonomic knowledge of all preservation states occurring at a site and in different depositional settings. However, this study, as well as previous studies [29–31,74], indicate characteristic CL spectra according to their host rocks. These differences can be characterized as follows:

1. Petrified wood preserved in pyroclastic rocks (Figure 14):
 - (a) multiphase (Figure 14a). First phase with yellow and/or red CL; second phase with blue CL. Both phases do not differ in anatomical preservation. Additionally, the first phase is replaced by, or even interspersed with the second phase. Anatomical preservation ranges from poorly preserved to well-preserved, with moderate to high preservation quality on average. Examples: Wendishain, Flöha (both this study), Chemnitz [29], petrified woods from tuffs intercalated in the žaltman Arkoses/Czech Republic [31].
 - (b) monophase (Figure 14d), promoted by short-lived blue CL.
2. Petrified wood preserved in epiclastic rocks (Figure 14): two subtypes:
 - (c) multiphase (Figure 14b). First phase with yellow and red CL; second phase with blue CL. Both phases differ remarkably in anatomical preservation, i.e., the second phase is accompanied by poor preservation of the corresponding wood. Anatomical preservation in the same range as (1). Example: Winnweiler (this study).
 - (d) monophase (Figure 14e), promoted by time-dependent blue-red CL. CL intensity conspicuously low. Example: petrified woods buried in-situ in epiclastic fluvial deposits of the Triassic Fremouw Formation/Antarctica [31] and Winnweiler.
3. Petrified wood preserved in siliciclastic rocks (Figure 14): two subtypes:
 - (e) multiphase (Figure 14c). First phase with yellow CL; second phase with blue CL. Both phases differ remarkably in anatomical preservation, i.e., the second phase is accompanied by poor preservation of the corresponding wood. Anatomical preservation ranges from poorly to moderately preserved, but is generally lower than in (1) and (2). Examples: Kyffhäuser, Wettin, Siebigerode (all this study).
 - (f) monophase (Figure 14f), promoted by time-dependent blue-red CL; in places accompanied with yellow CL. CL intensity conspicuously low. Broad range of anatomical preservation, ranging from moderate to high (including permineralizations with preservation of different intracellular fungi, [65,66]). Examples: Manebach, Crock (both this study), Balka/Czech Republic, petrified plants from the štikov Arkoses/Czech Republic and Tocantins/Brazil (the latter three in [31]).

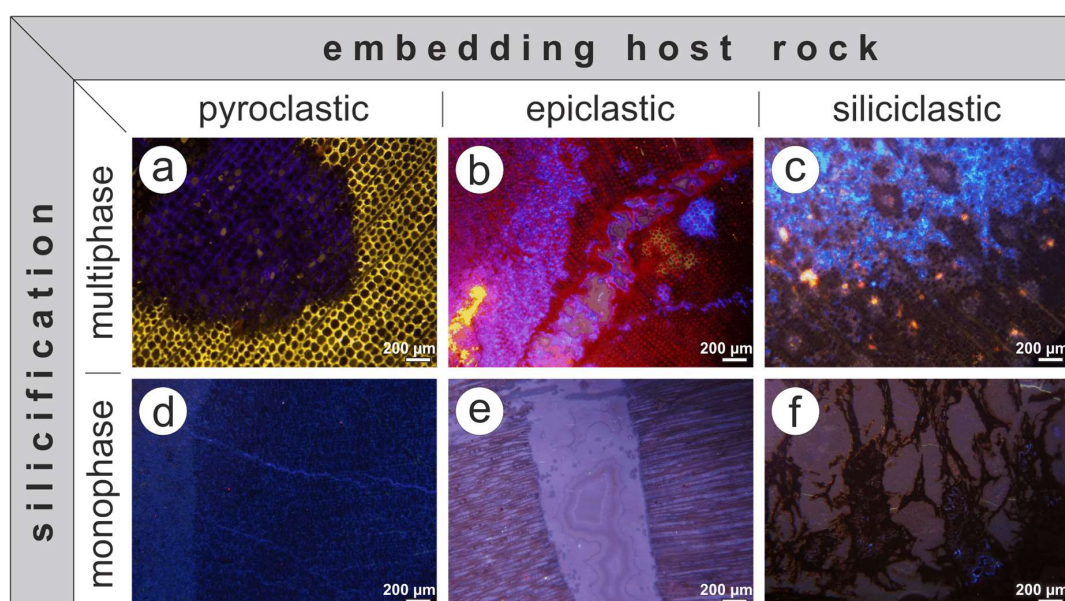


Figure 14. CL types of anatomically preserved (silicified) wood from the late Paleozoic of Central Europe based on [29–31,74], and this study. (a) Multiphase-pyroclastic type (K4815 from Chemnitz). Note replacement of primary yellow/red CL by blue CL. (b) Multiphase-epiclastic type (K6556 from Winnweiler). Note the reduced anatomical preservation in areas of blue CL. (c) Multiphase-siliciclastic type (K2097 from the Kyffhäuser). Note the generally low preservation quality and yellow CL of the initially silicified wood. (d) Monophase-pyroclastic type (K6573 from Flöha). (e) Monophase-epiclastic type (K6404 from Winnweiler). Note the homogeneous, initially blue CL. (f) Monophase-siliciclastic type (K6561 from Crock).

Based on the previous classification, multiphase and monophase silicifications occur in each type of embedding host rock (Figure 14). Accordingly, silicification can be accomplished stepwise (multiphase) or rapidly and completely (monophase) from the beginning.

Focusing on multiphase silicifications, differences with respect to the host rock comprise of (1) the CL colors occurring in the initial phase of silicification, and (2) the timing and process of second-phase silicification. Regarding the first point, red CL is only detected in petrified woods embedded in volcanoclastic deposits (Figures 9c,d and 14a,b), [30,74] described red CL in initially-silicified parts of the wood from the latest Pennsylvanian fluvial Žaltman Arkoses of the Intrasudetic Basin. However, [31] specified this occurrence later as being embedded in tuffs (Table 1). Additionally, all finds showing a red CL were made in recent streams and colluvial deposits lacking their exact stratigraphic occurrence. Hence, there is no example to date for initially formed red CL in anatomically preserved plants embedded in siliciclastic rocks.

Concerning the timing of second-phase silicification: In case of woods embedded in epiclastic and siliciclastic rocks, an interruption of silicification is indicated by poor preservation of wood showing blue CL (Figure 7f, 9f and Figure 11f). This break was apparently accompanied by ongoing degradation. Woods embedded in pyroclastic rocks, by contrast, show almost no differences in anatomical preservation between primarily and secondarily silicified parts (Figure 7d,f). Here, a hydrothermal overprint probably occurred in close succession to the initial silicification. Moreover, replacement of yellow and red CL by blue CL proves an originally complete silicification of the wood during the initial phase of silicification. However, with decreasing content of volcanic material in the embedding rocks, anatomical preservation decreases and the time interval between initial and final silicification increases. This relation could be caused by the fact that volcanogenic material is capable of producing high amounts and concentrations of silica within a short time span. Accordingly, silicification rate is enhanced favoring a rapid and complete silicification.

Monophase silicifications can consist of short-lived blue CL or homogeneous, low-intense, time-dependent CL. Both are due to early silicification promoted by hydrothermal fluids. Given the results, this CL type can be found in almost all host rocks and, thus, might be connected to different processes. In the case of Manebach and Crock, silica precipitation accompanied by time-dependent CL was obviously caused by volcanic activity, i.e., silica-bearing springs. Temperatures were low regarding well-preserved tissues of the permineralized stems including their endophytic biota. Litho- and biofacies of the Manebach Formation in general point to environments unfavorable for stromatolite formation, e.g., moderate to high rates of siliciclastic deposition and abundant metazoans in a differentiated ecosystem [64,75–77]. Hence, silica-bearing springs could represent niches for stromatolites. However, the results reflect an early rapid silicification for both Manebach and Crock, which is regarded here as being responsible for the preservation of organic tissues. This conclusion is supported by the latest studies on permineralizations [11].

6. Conclusions

Since 2000, several studies have demonstrated the vital contribution of CL microscopy in elucidating the diverse processes of wood silicification. In particular, CL has become a powerful tool in revealing silicification steps, as well as the physicochemical conditions of silica precipitation based on the visualization of lattice defects in the corresponding silica phases.

Results of the present study emphasize the use of multidisciplinary approaches, but offer the following suggestions for further petrified wood research:

- Interpreting the silicification of anatomically preserved wood requires a well-established knowledge of the geological background and stratigraphy, the mineralogy of the wood-bearing host rocks, and possible diagenetic influences.
- CL features and spectra of corresponding silica phases are indispensable to decipher the pathways of silicification and to reveal primary and secondary processes. Features like corroded detrital quartz in siliciclastic host rocks reflect diagenetic overprints capable of providing and/or dissolving silica. Hence, diagenetic processes might be reflected in the CL properties of petrified wood and can indicate possible secondary hydrothermal silicification.
- By now, CL replacement patterns were only observed in petrified woods embedded in ignimbrites. However, such patterns are missing in epiclastic deposits rich in volcanogenic components. Further research is necessary to verify this observation. A possible factor responsible for replacements during silicification of wood could be the temperature, which can be much higher in ignimbrites than in epiclastic/siliciclastic rocks.

The complexity and variability of CL features in silicified wood detected in this and previous studies emphasize the necessity of identifying CL patterns useful for reconstructing silicification processes. This concern not only refers to comparative studies of several localities from different depositional environments, but also demands for more detailed investigations of each single occurrence. In situ preserved T⁰ assemblages, for instance, like the early Permian Chemnitz Fossil Forest, are known to deliver different preservational forms occurring in various stacked host rocks [78]. However, petrified wood CL offers the possibility of distinguishing in which host rock the silicification took place. Steps of silicification can be revealed and described based on specific CL patterns observed in the corresponding silica phases. Additionally, this study has demonstrated that only a combination of paleobotanical and taphonomical features with CL patterns and spectra in petrified wood is crucial for a single occurrence. A site-specific “taphonomic fingerprint” based on CL patterns could break new grounds in petrified wood analysis, e.g., provenance studies of anatomically preserved plants found as reworked clasts in fluvial or glacial deposits.

Author Contributions: Investigation: S.T.; methodology: J.G.; project administration: S.T.; supervision: R.R.; visualization: S.T.; writing—original draft: S.T.; writing—review and editing: R.R. and J.G.

Funding: This research was funded by the Deutsche Forschungsgemeinschaft (DFG grant RO 1273/4-1 to RR).

Acknowledgments: We are grateful to Manfred Barthel, Stephan Schultka, both Berlin, and Robert Noll, Tiefenthal, Frank Löcse, St. Egidien, Ralf Puschmann, Frankenberg, and Jörg W. Schneider, Freiberg, for useful discussion and providing crucial specimens and photos. Special thanks are dedicated to Michael Magnus, Gudrun Geyer, Ronny Ziesemann, and Anja Obst, Freiberg, for thin section preparation. Reinhard Kleeberg, Freiberg, benefited the study with clay mineral analytics. Mathias Merbitz, Chemnitz, Anne Förster, and Marcel Hübner, both Freiberg, supported the preparation of the investigation material. We thank Jason A. Dunlop, Berlin, for linguistic corrections and the anonymous reviewers for their comprehensive help to improve the manuscript.

Conflicts of Interest: The authors declare no conflict of interest.

References

1. Dernbach, U.; Tidwell, W.D.I. *Secrets of Petrified Plants—Fascination from Millions of Years*; D'ORO Publishers: Heppenheim, Germany, 2002; p. 232. ISBN 978-3932181047.
2. Daniels, F.J.; Dayvault, R.D. *Ancient Forests. A Closer Look at Fossil Wood*; Western Colorado Publishing Company: Grand Junction, CO, USA, 2006; p. 450. ISBN 978-0966293814.
3. Schüssler, H.; Simon, T. *Aus Holz Wird Stein. Kieselhölzer aus Dem Keuper Frankens*; Verlag und Offsetdruck Eppe GmbH: Aulendorf, Germany, 2007; p. 192. ISBN 978-3890890913.
4. Niemirowska, A. *Skamieniale Drewno Drzew Gatunków Lisciastych, Iglastyh Oraz Paproci*; Wydawnictwo Poligraf: Brzezia Łaka, Poland, 2013; p. 384. ISBN 978-8378560838.
5. Kerp, H. Organs and tissues of Rhynie chert plants. *Philos. Trans. R. Soc. B* **2017**, *373*. [[CrossRef](#)] [[PubMed](#)]
6. Akahane, H.; Furuno, T.; Miyama, H.; Yoshikawa, T.; Yamamoto, S. Rapid wood silicification in hot spring water: An explanation of silicification of wood during the Earth's history. *Sediment. Geol.* **2004**, *169*, 219–228. [[CrossRef](#)]
7. Rößler, R.; Zierold, T.; Feng, Z.; Kretschmar, R.; Merbitz, M.; Annacker, V.; Schneider, J.W. A snapshot of an early Permian ecosystem preserved by explosive volcanism: New results from the Chemnitz Petrified Forest, Germany. *Palaios* **2012**, *27*, 814–834. [[CrossRef](#)]
8. Philippe, M.; Boonchai, N.; Ferguson, D.K.; Hui, J.; Songtham, W. Giant trees from the Middle Pleistocene of Northern Thailand. *Quat. Sci. Rev.* **2013**, *65*, 1–4. [[CrossRef](#)]
9. Mustoe, G.E.; Acosta, M. Origin of petrified wood color. *Geosciences* **2016**, *6*, 25. [[CrossRef](#)]
10. Mustoe, G.E. Late Tertiary Petrified Wood from Nevada, USA: Evidence of multiple silicification pathways. *Geosciences* **2015**, *5*, 286–309. [[CrossRef](#)]
11. Mustoe, G.E. Wood Petrification: A New View of Permineralization and Replacement. *Geosciences* **2017**, *7*, 119. [[CrossRef](#)]
12. St. John, R.N. Replacement vs. impregnation in petrified wood. *Econ. Geol.* **1927**, *22*, 729–739. [[CrossRef](#)]
13. Buurman, P. Mineralization of fossil wood. *Scr. Geol.* **1972**, *12*, 1–35.
14. Leo, R.F.; Barghoorn, E.S. Silicification of wood. *Harvard Univ. Bot. Mus. Leaflet.* **1976**, *25*, 1–47.
15. Sigleo, A.C. Geochemistry of silicified wood and associated sediments, Petrified Forest National Monument, Arizona. *Chem. Geol.* **1979**, *26*, 151–163. [[CrossRef](#)]
16. Ballhaus, C.T.; Gee, K.; Greef, K.; Bockrath, C.; Mansfield, T.; Rhede, D. The silicification of trees in volcanic ash: An experimental study. *Geochim. Cosmochim. Acta* **2012**, *84*, 62–74. [[CrossRef](#)]
17. Hellowell, J.; Balhaus, C.; Gee, C.T.; Mustoe, G.E.; Nagel, T.J.; Wirth, R.; Rethemeyer, J.; Tomaschek, F.; Geisler, T.; Greef, K.; Mansfeldt, T. Incipient silicification of recent conifer wood at a Yellowstone hot spring. *Geochim. Cosmochim. Acta* **2015**, *149*, 79–87. [[CrossRef](#)]
18. Dietrich, D.; Viney, M.; Lampke, T. Petrifications and wood-templated ceramics: Comparisons between natural and artificial silicification. *IAWA J.* **2015**, *36*, 167–185. [[CrossRef](#)]
19. Channing, A.; Edwards, D. Experimental silicification of plants in Yellowstone hot-spring environments. *Trans. R. Soc. Edinb. Earth Sci.* **2004**, *94*, 503–521. [[CrossRef](#)]
20. Channing, A.; Edwards, D. Wetland megabias: Ecological and ecophysiological filtering dominates the fossil record of hot spring floras. *Palaeontology* **2013**, *56*, 523–556. [[CrossRef](#)]
21. Dietrich, D.; Lampke, T.; Rößler, R. Microstructure study on silicified wood from the Permian Petrified Forest of Chemnitz. *Paläontol. Z.* **2013**, *87*, 397–407. [[CrossRef](#)]
22. Sippel, R.F. Sandstone petrology, evidence from luminescence petrography. *J. Sediment. Petrol.* **1968**, *38*, 530–554. [[CrossRef](#)]

23. Götze, J.; Plötze, M.; Habermann, D. Origin, spectral characteristics and practical applications of the cathodoluminescence (CL) of quartz: A review. *Mineral. Petrol.* **2001**, *71*, 225–250. [[CrossRef](#)]
24. Richter, D.K.; Götze, T.; Götze, J.; Neuser, R.D. Progress in application of cathodoluminescence (CL) in sedimentary petrology. *Mineral. Petrol.* **2003**, *79*, 127–166. [[CrossRef](#)]
25. Götze, J. Chemistry, textures and physical properties of quartz—Geological interpretation and technical application. *Mineral. Mag.* **2009**, *73*, 645–671. [[CrossRef](#)]
26. Zinkernagel, U. Cathodoluminescence of quartz and its application to sandstone petrology. *Contrib. Sedimentol.* **1978**, *8*, 1–69.
27. Ramseyer, K.; Baumann, J.; Matter, A.; Mullis, J. Cathodoluminescence colours of alpha-quartz. *Mineral. Mag.* **1988**, *52*, 669–677. [[CrossRef](#)]
28. Ramseyer, K.; Mullis, J. Factors influencing short-lived blue cathodoluminescence of alpha quartz. *Am. Mineral.* **1990**, *75*, 791–800.
29. Götze, J.; Rößler, R. Kathodolumineszenz-Untersuchungen an Kieselhölzern—I. Silifizierungen aus dem Versteinerten Wald von Chemnitz (Perm, Deutschland). *Veröff. Mus. Naturkunde Chemnitz* **2000**, *23*, 35–50.
30. Matysova, P.; Leichmann, J.; Grygar, T.; Rößler, R. Cathodoluminescence of silicified trunks from the Permo-Carboniferous basins in eastern Bohemia, Czech Republic. *Eur. J. Mineral.* **2008**, *20*, 217–231. [[CrossRef](#)]
31. Matysová, P.; Rössler, R.; Götze, J.; Leichmann, J.; Forbes, G.; Taylor, E.L.; Sakala, J.; Grygar, T. Alluvial and volcanic pathways to silicified plant stems (Upper Carboniferous-Triassic) and their taphonomic and palaeoenvironmental meaning. *Palaeogeogr. Palaeoclimatol. Palaeoecol.* **2010**, *292*, 127–143. [[CrossRef](#)]
32. Matysová, P.; Booi, M.; Crow, M.C.; Hasibuan, F.; Perdono, A.P.; Van Waveren, I.M.; Donovan, S.K. Burial and preservation of a fossil forest on an early Permian (Asselian) volcano (Merangin River, Sumatra, Indonesia). *Geol. J.* **2017**, *154*, 1–19. [[CrossRef](#)]
33. Götze, J.; Plötze, M.; Fuchs, H.; Habermann, D. Defect structure and luminescence behaviour of agate: Results of electron paramagnetic resonance (EPR) and cathodoluminescence (CL) studies. *Mineral. Mag.* **1999**, *63*, 149–163. [[CrossRef](#)]
34. Götze, J.; Pan, Y.; Stevens-Kalceff, M.; Kempe, U.; Müller, A. Origin and significance of the yellow cathodoluminescence (CL) of quartz. *Am. Mineral.* **2015**, *100*, 1469–1482. [[CrossRef](#)]
35. Rößler, R.; Zierold, T. Back to the roots of palaeobotany—Chemnitz and its palaeontological collection. In *Paleontological Collections of Germany, Austria and Switzerland*; Beck, L.A., Joger, U., Eds.; Springer International Publishing: Cham, Switzerland, 2018; ISBN 978-3-319-77400-8.
36. Schneider, J.W.; Werneburg, R.; Rößler, R.; Voigt, S.; Scholze, F. Example for the description of basins in the CPT Nonmarine-Marine Correlation Chart Thuringian Forest Basin, East Germany. *Permophiles* **2015**, *61*, 29–35.
37. Neuser, R.D.; Bruhn, F.; Götze, J.; Habermann, D.; Richter, D.K. Kathodolumineszenz: Methodik und Anwendung. *Zentral. Geol. Paläontol.* **1995**, *1*, 287–306.
38. DiMichele, W.A.; Aronson, R.B. The Pennsylvanian-Permian vegetational transition: A terrestrial analogue to the onshore-offshore hypothesis. *Evolution* **1992**, *46*, 807–824. [[CrossRef](#)] [[PubMed](#)]
39. DiMichele, W.A.; Pfefferkorn, H.W.; Gastaldo, R.A. Response of late Carboniferous and early Permian plant communities to climate change. *Annu. Rev. Earth Planet. Sci.* **2001**, *29*, 461–487. [[CrossRef](#)]
40. McCann, T.; Pascal, C.; Timmermann, M.J.; Krzywiec, P.; López-Gómez, J.; Wetzel, A.; Krawczyk, C.M.; Rieke, H.; Lamarche, J. Post-Variscan (end Carboniferous–Early Permian) basin evolution in Western and Central Europe. In *European Lithosphere Dynamics*; Gee, G., Stephenson, R.A., Eds.; Geological Society Memoir No. 32; Geological Society: London, UK, 2006; pp. 355–388. ISBN 9781 86239 212 0.
41. Kroner, U.; Romer, R.L. Two plates—Many subduction zones: The Variscan orogeny reconsidered. *Gondwana Res.* **2013**, *24*, 298–329. [[CrossRef](#)]
42. Schulmann, K.; Schaltegger, U.; Jezek, J.; Thompson, A.B.; Edal, J.-B. Rapid burial and exhumation during orogeny: Thickening and synconvergent exhumation of thermally weakened and thinned crust (Variscan Orogen in Western Europe). *Am. J. Sci.* **2002**, *302*, 856–879. [[CrossRef](#)]
43. Rößler, R.; Barthel, M. Rotliegend taphocoenoses preservation favoured by rhyolitic explosive volcanism. *Freib. Forsch.* **1998**, *C474*, 59–101.
44. Luthardt, L.; Rößler, R.; Schneider, J.W. Palaeoclimatic and site-specific conditions in the early Permian fossil forest of Chemnitz—Sedimentological, geochemical and palaeobotanical evidence. *Palaeogeogr. Palaeoclimatol. Palaeoecol.* **2016**, *441*, 627–652. [[CrossRef](#)]

45. Roscher, M.; Schneider, J.W. Permo-Carboniferous climate: Early Pennsylvanian to Late Permian climate development of central Europe in a regional and global context. In *Non-Marine Permian Biostratigraphy and Biochronology*; Lucas, S.G., Cassinis, G., Schneider, J.W., Eds.; Geological Society London Special Publications: London, UK, 2006; Volume 265, pp. 95–136.
46. Schneider, J.W.; Körner, F.; Roscher, M.; Kroner, U. Permian climate development in the northern peri-Tethys area—The Lodève basin, French Massif Central, compared in a European and global context. *Palaeogeogr. Palaeoclimatol. Palaeoecol.* **2006**, *240*, 161–183. [[CrossRef](#)]
47. Barthel, M. *Die Rotliegendflora des Thüringer Waldes*; Naturhist. Mus. Schleusingen: Schleusingen, Germany, 2009; p. 170.
48. Schneider, J.W.; Romer, R.L. The late Variscan molasses (late Carboniferous to late Permian) of the Saxo-Thuringian Zone. In *Pre-Mesozoic Geology of Saxo-Thuringia—From the Cadomian Active Margin to the Variscan Orogen*; Linnemann, U., Romer, R.L., Eds.; E. Schweizerbart'sche Verlagsbuchhandlung: Stuttgart, Germany, 2010; pp. 323–346. ISBN 3510652592.
49. Löcse, F.; Meyer, J.; Klein, R.; Linnemann, U.; Weber, J.; Rößler, R. Neue Florenzfunde in einem Vulkanit des Oberkarbons von Flöha—Querschnitt durch eine ignimbritische Abkühlungseinheit. *Veröff. Mus. Naturkunde Chemnitz* **2013**, *36*, 85–142.
50. Löcse, F.; Linnemann, U.; Schneider, G.; Annacker, V.; Zierold, T.; Rößler, R. 200 Jahre *Tubicaulis solenites* (Sprengel) Cotta—Sammlungsgeschichte, Paläobotanik und Geologie eines oberkarbonischen Baumfarn-Unikats aus dem Schweddey-Ignimbrit vom Gückelsberg bei Flöha. *Veröff. Mus. Naturkunde Chemnitz* **2015**, *38*, 5–46.
51. Löcse, F.; Zierold, T.; Rößler, R. Provenance and collection history of *Tubicaulis solenites* (Sprengel) Cotta—A unique fossil tree fern and its 200-year journey through the international museum landscape. *J. Hist. Collect.* **2018**, *30*, 241–251. [[CrossRef](#)]
52. Gothan, W. Die Altersstellung des Karbons von Flöha i. Sa. im Karbonprofil auf Grund der Flora. *Abh. Sächs. Geol. Landesamt* **1932**, *12*, 5–16.
53. Walter, H.; Rößler, R. Ein großer Kieselholz-Stamm aus dem Rotliegend Sachsens (Kohren-Formation, Nordwestsächsische Senke). *Veröff. Mus. Naturkunde Chemnitz* **2006**, *29*, 177–188.
54. Röllig, G. Zur Petrogenese und Vulkanotektonik der Pyroxenquarzporphyre (Ignimbrite) des Nordsächsischen Vulkanitkomplexes. *Jahrb. Geol.* **1976**, *5/6*, 175–268.
55. Walter, H. Rotliegend im Nordwestsächsischen Becken. In *Stratigraphie von Deutschland X. Rotliegend. Teil I: Innervariscische Becken*; Lützner, H., Kowalczyk, G., Eds.; E. Schweizerbart'sche Verlagsbuchhandlung: Stuttgart, Germany, 2012; pp. 517–529. ISBN 3510492250.
56. Haneke, J.; Lorenz, V.; Stollhofen, H. Donnersberg-Formation. In *Stratigraphie Von Deutschland X. Rotliegend. Teil I: Innervariscische Becken*; Lützner, H., Kowalczyk, G., Eds.; E. Schweizerbart'sche Verlagsbuchhandlung: Stuttgart, Germany, 2012; pp. 254–377. ISBN 3510492250.
57. Lorenz, V.; Haneke, J. Relationship between diatremes, dykes, sills, laccoliths, intrusive-extrusive domes, lava flows, and tephra deposits with unconsolidated water-saturated sediments in the late Variscan intermontane Saar-Nahe Basin, SW Germany. *Geol. Soc. Lond. Spec. Publ.* **2004**, *234*, 75–124. [[CrossRef](#)]
58. Charpentier, J.F.W. *Mineralogische Geographie der Chursächsischen Lande Mit Kupfern*; Verlag Siegfried Lebrecht Crusius: Leipzig, Germany, 1778; p. 432.
59. Trümper, S.; Rößler, R. Neues vom Kyffhäuser: Geologische Untersuchungen erhellen die Taphonomie vom Wald zum Holzlagerplatz (Oberkarbon, N-Thüringen). *Geowiss. Mitt.* **2017**, *67*, 20–21.
60. Mägdefrau, K. Die Kieselhölzer im obersten Oberkarbon des Kyffhäusergebirges. *Ber. Deutsch. Bot. Ges.* **1958**, *71*, 133–142.
61. Meister, J. Sedimentpetrographische und lithologische Untersuchungen im Siles des Kyffhäusers. *Hallesches Jahrb. Mitteldtsch. Erdgesch.* **1967**, *9*, 75–92.
62. Schneider, J.W.; Rößler, R.; Gaitzsch, B.G.; Gebhardt, U.; Kampe, A. Saale-Senke. In *Stratigraphie von Deutschland X. Rotliegend. Teil I: Innervariscische Becken*; Lützner, H., Kowalczyk, G., Eds.; E. Schweizerbart'sche Verlagsbuchhandlung: Stuttgart, Germany, 2012; pp. 447–460. ISBN 3510492250.
63. Lützner, H. Sedimentologie der Manebach-Formation in den fossilführenden Aufschlüssen bei Manebach. *Beitr. Geol. Thüring.* **2001**, *8*, 67–91.

64. Lützner, H.; Andreas, D.; Schneider, J.W.; Voigt, S.; Werneburg, W. Stefan und Rotliegend im Thüringer Wald und seiner Umgebung. In *Stratigraphie von Deutschland X. Rotliegend. Teil I: Innersarische Becken*; Lützner, H., Kowalczyk, G., Eds.; E. Schweizerbart'sche Verlagsbuchhandlung: Stuttgart, Germany, 2012; pp. 418–487. ISBN 3510492250.
65. Barthel, M.; Krings, M.; Rößler, R. Die schwarzen Psaronien von Manebach, ihre Epiphyten, Parasiten und Pilze. *Semana* **2010**, *25*, 41–60.
66. Krings, M.; Harper, C.J.; White, J.F.; Barthel, M.; Heinrichs, J.; Taylor, E.L.; Taylor, T.N. Fungi in a *Psaronius* root mantle from the Rotliegend (Asselian, Lower Permian) of Thuringia, Germany. *Rev. Palaeobot. Palynol.* **2017**, *239*, 14–30. [[CrossRef](#)]
67. Noll, R.; Rößler, R.; Wilde, V. 150 Jahre Dadoxylon. Zur Anatomie fossiler Koniferen- und Cordaitenhölzer aus dem Rotliegend des euramerischen Florengebietes. *Veröffentlichungen des Museums für Naturkunde* **2005**, *28*, 29–48.
68. Heaney, P.J. A proposed mechanism for the growth of chalcedony. *Contrib. Mineral. Petrol.* **1993**, *115*, 66–74. [[CrossRef](#)]
69. Götze, J.; Möckel, R.; Langhof, N.; Hengst, M.; Klinger, M. Silicification of wood in the laboratory. *Ceram. Silik.* **2008**, *52*, 268–277.
70. Owen, M.R. Radiation-damage halos in quartz. *Geology* **1988**, *16*, 529–532. [[CrossRef](#)]
71. Meunier, J.D.; Sellier, E.; Pagel, M. Radiation-damage rims in quartz from uranium-bearing sandstones. *J. Sediment. Petrol.* **1990**, *60*, 53–58. [[CrossRef](#)]
72. Kremer, B.; Kazmierczak, J.; Łukomska-Kowalczyk, M.; Kempe, S. Calcification and silicification: Fossilization potential of cyanobacteria from stromatolites of Niuafou'u's Caldera Lakes (Tonga) and implications for the early fossil record. *Astrobiology* **2012**, *12*, 535–548. [[CrossRef](#)] [[PubMed](#)]
73. Barthel, M. Pflanzengruppen und Vegetationseinheiten der Manebach-Formation. *Beitr. Geol. Thüring.* **2001**, *8*, 93–123.
74. Mencl, V.; Matysová, P.; Sakala, J. Silicified wood from the Czech part of the Intra Sudetic Basin (Late Pennsylvanian, Bohemian Massif, Czech Republic): Systematics, silicification, and palaeoenvironment. *Neues Jahrb. Geol. Paläontol. Abh.* **2009**, *253*, 269–288. [[CrossRef](#)]
75. Pratt, B.R. Stromatolite decline—A reconsideration. *Geology* **1982**, *10*, 512–515. [[CrossRef](#)]
76. Werneburg, R. Ein See-Profil aus dem Unter-Rotliegend des (Unter-Perm) von Manebach (Thüringer Wald). *Veröff. Naturhist. Mus. Schleus.* **1997**, *12*, 63–67.
77. Werneburg, R. Ein Pelycosaurier aus dem Rotliegend des Thüringer Waldes. *Veröff. Naturhist. Mus. Schleus.* **1999**, *14*, 55–58.
78. Luthardt, L.; Hofmann, M.; Linnemann, U.; Gerdes, A.; Marko, L.; Rößler, R. A new U-Pb zircon age and a volcanogenic model for the early Permian Chemnitz Fossil Forest. *Int. J. Earth Sci.* **2018**, *107*, 2465–2489. [[CrossRef](#)]

